

# Magnetically Enhanced Microflow Cytometer for Bead-based Immunoaffinity Measurements in Whole Blood Samples



Scientific thesis for the attainment of the academic degree  
Master of Science (M.Sc.)  
of the Department of Electrical and Computer Engineering  
at the Technical University of Munich.

**Supervised by** Dr.-Ing. Mathias Reisbeck  
Prof. Dr. rer. nat. Oliver Hayden

**Submitted by** Johann Alexander Brenner  
Weisbergerstraße 5a  
85053 Ingolstadt  
03662733

**Submitted on** December 4<sup>th</sup>, 2020 at Munich

# Contents

<b>1 Abstract .....</b>	<b>4</b>
<b>2 Theory .....</b>	<b>5</b>
2.1 Microfluidics .....	5
2.1.1 Approximating the Navier-Stokes-Equation .....	5
2.1.2 Flow and Shear in Microchannels with fiscous Vluids .....	6
2.1.3 Force Equilibrium of Microbeads .....	7
2.2 Surface Chemistry .....	9
2.2.1 Surface Oxidation Methods.....	9
2.2.2 Silane Chemistry .....	13
2.2.3 Carbodiimide Crosslinker Chemistry .....	14
2.2.4 Microscopic Particle Surface Physics .....	16
2.2.5 The Biotin-Avidin-System .....	16
2.3 Magnetoresistive Sensing .....	16
<b>3 Materials and Methods .....</b>	<b>17</b>
3.1 Magnetic Sensor Device .....	17
3.1.1 Assembly of Sensor.....	17
3.1.2 Design and Fabrication of Microfluidics .....	17
3.1.3 Peripheral Components and Optical Readout.....	19
3.2 Magnetic Beadometry .....	22
3.2.1 Bead Capture Assay .....	22
3.3 Surface Bio-Functionalization .....	23
3.3.1 Surface Activation.....	23
3.3.2 Chemical Surface Functionalization .....	24
3.3.3 Surface Bioconjugation .....	25
3.3.4 Particle Functionalization.....	26
<b>4 Results .....</b>	<b>30</b>
4.1 Virtual Prototyping of Cell Signals .....	30
4.1.1 Numerical investigation of immunomagnetic label density and size on quantitative magnetoresistive sensing of single cells and cell aggregates .....	30
4.1.2 Single Cell Signal .....	30

4.1.3	Cell Aggregates .....	30
4.2	Reference Bead Surface Functionalization.....	30
4.2.1	Amine-Surface Biotinylation .....	30
4.2.2	Carboxy-Surface Biotinylation .....	35
4.2.3	Surface Magnetization of Biofunctionalized Beads .....	35
4.3	Concentration Measurements in MRCyte.....	35
4.3.1	Count Stability.....	35
4.3.2	Calibration of Flow Field .....	35
4.3.3	Differential Counting Setup .....	35
4.4	Surface Modification and Biofunctionalization of the Sensor Chip Substrate	37
4.4.1	Physisorption .....	37
4.4.2	Covalent Attachment.....	38
<b>5</b>	<b>Discussion.....</b>	<b>40</b>
<b>6</b>	<b>Outlook.....</b>	<b>41</b>
	<b>List of Abbreviations.....</b>	<b>44</b>
	<b>List of Figures .....</b>	<b>47</b>
	<b>List of Tables .....</b>	<b>48</b>
	<b>Bibliography .....</b>	<b>50</b>
	<b>Statement .....</b>	<b>65</b>

# 1. Abstract

## 2. Theory

The main measurement principle by a giant magneto resistance (GMR)-Sensor has been already described and characterized exhaustively by Helou [1], Reisbeck [2] and Brenner [3]. Therefore, this theoretical part will focus on (bio-)physical aspects of a cell rolling motion inside a microfluidic channel and surface modification chemistry.

### 2.1. Microfluidics

en Standardumfang wählen, Re, Navier Stokes, Scherraten, nicht newtonsche / newtonsche Fluide)

#### 2.1.1. Approximating the Navier-Stokes-Equation

The main experiments of this work were carried out in microfluidic environments, which exhibit favorable properties compared to common turbulent systems. From a fluid-mechanical standpoint, shrinking the scales makes interfacial as well as electrokinetic phenomena much more significant, and reduces the importance of pressure and gravity.[4] However, electrodynamics, chemistry and fluid dynamics are inextricably intertwined, so that fluid flow can create electric fields (and vice versa), with a degree of coupling driven by the surface chemistry. Many of the resulting phenomena arise or can be explained by Cauchy-Momentum equation (eq. 2.3) and the resulting Navier-Stokes equation for incompressible fluids (eq. 2.4).

$$\frac{\partial}{\partial t} \iiint \rho dV = - \iint \rho \mathbf{u} \cdot \vec{n} dA \quad (2.1)$$

$$\nabla \cdot \mathbf{u} = 0 \quad (2.2)$$

$$\rho \frac{\partial \mathbf{u}}{\partial t} + \rho \mathbf{u} \cdot \nabla \mathbf{u} = \nabla \cdot \boldsymbol{\tau} + \sum_i \mathbf{f}_i \quad (2.3)$$

$$\underbrace{\rho \frac{\partial \mathbf{u}}{\partial t}}_{\text{Transient}} + \underbrace{\rho \mathbf{u} \cdot \nabla \mathbf{u}}_{\text{Convection}} = \underbrace{-\nabla p}_{\text{Pressure}} + \underbrace{\eta \nabla^2 \mathbf{u}}_{\text{Viscous}} + \underbrace{\sum_i \mathbf{f}_i}_{\text{Body Forces}} \quad (2.4)$$

conservation of mass, momentum reynolds number

### 2.1.2. Flow and Shear in Microchannels with viscous Fluids

The foremost characteristic of a microchannel is the laminar flow behavior, which causes deterministic pathlines. Mathematically, this is described by the reynolds number, which compares the inertia to shear forces. If it results below a certain threshold of 2000, laminar flow can be assumed. This holds true for the utilized microfluidic with the dimensions  $12\,000\,\mu\text{m} \times 700\,\mu\text{m} \times 150\,\mu\text{m}$  ( $l \times w \times h$ ) and aqueous buffer solutions, where the channel width was used as characteristic length  $l$ . Hence, simplifications of the Navier-Stokes equation can be applied to our system.

$$Re = \frac{2\rho|\bar{u}|l}{\eta} \quad (2.5)$$

The step from the Cauchy momentum equation to the Navier-Stokes equation is complex and harbors several sources of error. First, an incompressible newtonian fluid as well as channel is assumed. The used water suspensions can be approximated with negligible compressibility, which is not true for the real case. Also, for blood or other shear-thinning fluids some deviations are prone for high errors. This happens due to the fact that the surface stress tensor ( $\tau$ ) is decomposed into pressure and viscous contributions as shown in the equations 2.6. Then, the divergence relation of the respective viscous stress (eq. 2.7) does not hold for non-uniform viscosity  $\eta$ .

$$\tau = \tau_{viscous} + \tau_{pressure} = 2\eta\epsilon - p\mathbf{I}_{3\times 3} \quad (2.6)$$

$$\nabla \cdot \tau_{viscous} = \nabla \cdot 2\eta\epsilon = \nabla \cdot \eta\nabla\mathbf{u} \stackrel{\substack{\text{only if } \eta \\ \text{uniform}}}{=} \eta\nabla^2\mathbf{u} \quad (2.7)$$

Second, the channel height varies in reality as a result of fabrication inaccuracies. In the model case of a flow through a rectangular channel, no analytical solution of the Navier-Stokes equation exists, but a Fourier Series expansion if channel width is larger than channel height. [5] The equation 2.8 shows that height deviations can have prominent influence on a channel velocity simulation as it is proportional to  $h^2$ . Further, the flow rate (which is the velocity integral over the channel cross section) depends even on  $h^3$ .

$$u_x(y, z) = \frac{4h^2\Delta p}{\pi^3\eta l} \sum_{n,odd}^{\infty} \frac{1}{n^3} \left( 1 - \frac{\cosh(n\pi\frac{y}{h})}{\cosh(n\pi\frac{w}{2h})} \right) \sin(n\pi\frac{z}{h}) \quad (2.8)$$

Third, the transient term (eq. 2.4) was neglected in all simulations, but a connected syringe pump possesses a slow rise time (Fig. 1a) and a remaining “pulsation error” in

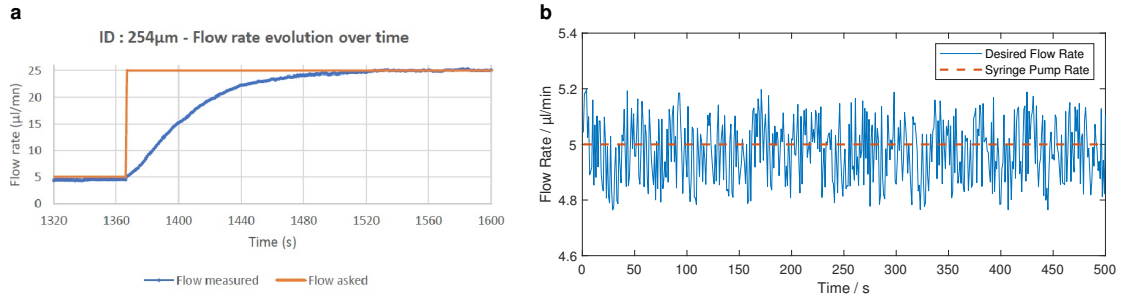


**Figure 1: Syringe Pump error sources**

Set flow rate: —, Real Flow Rate: — **a**, Transient step answer of a syringe pump through a microtube with 254  $\mu\text{m}$  inner diameter. **b**, Steady state flow rate error around the desired  $5 \mu\text{L min}^{-1}$  dispensing rate. A sinusoidal behaviour caused by the microstepping can be observed. [6]

steady state (Fig. 1b). In effect, another error adds to the simulation, which is only valid after several ten seconds of the last flow rate change.

For later studies in a matlab model, the flow velocity and shear stress computations were carried out with the error sources considered.

### 2.1.3. Force Equilibrium of Microbeads

Stokes Drag Force with lift correction Gravity Electro-static interaction Magnetic Force  
Friction Interface-Forces Faraus linquist Protein interaction/ Avidity,Affinity

### Rolling Motion of Beads

#### **2.1.4.**

## 2.2. Surface Chemistry

Introducing biological samples, such as peripheral whole blood and -plasma, into microsystems needs careful consideration of surface modification compared to buffered samples of adjusted pH containing cells or polymeric beads. Blood-material contact most often initiates surface-mediated reactions that lead to cell activation, blood clotting or biofilm formation. In order to minimize unspecific interactions on surfaces, most contact faces are passivated with chemically and biologically inert materials or even composed entirely from it. In any use case, where a surface has to be functionalized with biomolecules, the intrinsic inertness then requires specialized methods for permanent and reproducible adhesion.[7]

sources

Molecules can be immobilized through various mechanisms on surfaces to achieve a biological or chemical functionality. The most simple is physisorption. Here, a biomolecule is bonded only by weak elektrostatic, van-der-Waals or dipole-dipole interaction with a adsorption enthalpy below  $50 \text{ kJ mol}^{-1}$ . In contrast, this yields fast reaction rates, because no activation energy has to be overcome. Although a large number of molecules can be captured with this method, several drawbacks have been identified. [8], [9] For example, immobilized receptors can desorb or move inside the channel, which in turn reduces sensitivity or causes false-positive results. [10], [11]

source

Therfore, most functionalization approaches rely on chemisorption where molecules are covalently bound to a surface. Due to the higher activation energy barrier this bonding mechanism works slower in comparison to physisorption, though higher temperatures or catalysts can promote an equilibrium. One of the most well-known strategies to bring reproducible thin films on surfaces is the formation of self-assembled monolayers (SAMs) where a dense layer of single molecules with high internal order forms upon dipping into a surface-active substance. [12]

Sensitivity und  
False-Positive  
Results soll-  
ten hier kurz  
dargestellt wer-  
den, zumindest  
in der Anwen-  
dung.

### 2.2.1. Surface Oxidation Methods

Modifying a surface with functional silanes, requires oxidized sites, for example –OH (hydroxyl) resp. Si–OH (silanol) groups. In order to increase the presence of those reactive groups on substrates, various activation methods such as piranha, a mixture from hydrogen peroxide ( $\text{H}_2\text{O}_2$ ) and sulfuric acid ( $\text{H}_2\text{SO}_4$ ), oxygen gas ( $\text{O}_2$ ) - plasma treatment or an hydrofluoric acid (HF) dip can be chosen. [13]

Critical for any surface engineering is the internal structure and in consequence the binding energies of the surficial groups. The three mainly used substrates in this work, glass, poly(dimethyl siloxane) (PDMS) and silicon nitride ( $\text{Si}_3\text{N}_4$ ), contain highly conserved, homogeneous surfaces and are mostly well characterized. The surface of glass exhibits already silanol groups intrinsically and consequentially demands only a removal of impurities. PDMS and  $\text{Si}_3\text{N}_4$  however have different compositions as shown in Fig. 11 and 3 hence requiring a strong oxidation agents to completely exchange its interface. [14]–[16]

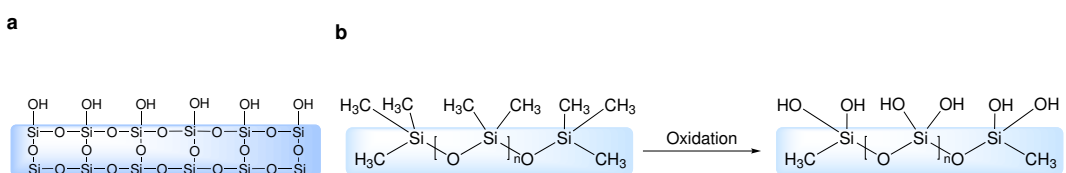
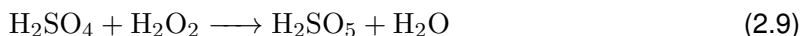


**Figure 2: Different substrate surfaces: glass and PDMS**

Surface groups and internal structure of quartz glass (a) and PDMS (b). After an oxidation step, the methyl groups are changed to hydroxyl.

### Piranha Solution

Piranha is an oxidizer composed of  $\text{H}_2\text{O}_2$  and  $\text{H}_2\text{SO}_4$ , typically in volume ratios between 1:3 and 1:7. The effectiveness of piranha in removing organic residues and creating hydroxyl groups is induced by two distinct processes. In the first process, which is notably faster, hydrogen and oxygen are removed as units of water by the concentrated  $\text{H}_2\text{SO}_4$ . (Reaction 2.9) This occurs due to the thermodynamically very favorable reaction with an enthalpy of  $-880 \text{ kJ mol}^{-1}$  and produces Caro's acid ( $\text{H}_2\text{SO}_5$ ), one of the strongest oxidants known. [17]



In another process the sulfuric acid boosts hydrogen peroxide from a mild oxidizer into the more aggressive atomic oxygen by the dehydration of  $\text{H}_2\text{O}_2$ . (Reaction 2.10) These two dehydration processes in the mixture result on the one hand in a highly corrosive nature against organic materials, particularly against the difficult to remove carbon. On

the other hand, it is strongly acidic and oxidizing which in turn requires great care and substantial safety measures to prepare and use it harmlessly.

### Hydrofluoric Acid

One of the used substrates in this work is  $\text{Si}_3\text{N}_4$  as passivation layer above magnetic sensors as it has a significant better diffusion barrier against water or sodium ions and is chemically very inert. [18]

However, due to its complex crystal structure it is also difficult to modify by common chemicals and the exact surface composition still subject to scientific discussion. [19] Apart from cleaning the surface with piranha, few other modification methods have been reported, but only one suitable for the direct generation of hydroxyl groups.

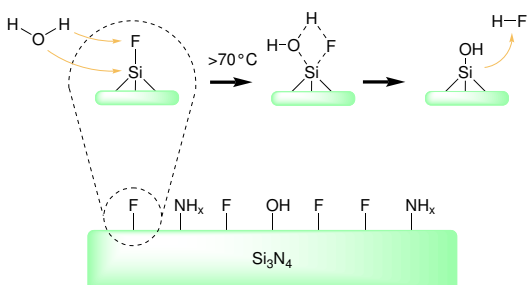


Figure 3: Proposed modification of  $\text{Si}_3\text{N}_4$  with HF

There, as depicted in 3, the reaction  $\text{Si}-\text{OH} + \text{HF} \leftrightarrow \text{Si}-\text{F} + \text{H}_2\text{O}$  takes place reversibly due to the coincidence that  $\text{Si}-\text{O}$  and  $\text{O}-\text{H}$  as well as  $\text{Si}-\text{F}$  and  $\text{H}-\text{F}$  bonds have similar binding energies and hence the forward and reverse reactions a low activation energy. After Le Chatelier's principle, a depletion of HF in the bulk leads then to an increase in surficial hydroxyl groups. [20] In further works, it has been determined that an oxidation with a similar protocol based on aqueous HF yields a variable  $\text{Si}-\text{O}-\text{Si}$  (siloxane) coverage with  $37 \pm 17\%$  of a monolayer, which nevertheless can be used for stable, covalent attachment of silanes. Nominally the same surface coverages of silicon oxide and nitride surfaces could be achieved by ethoxy- and chlorosilanization. [21] As shown by [22], the subsequent surfaces exhibit beneficial biological properties and can be modified by further standard procedures.

### Oxygen Plasma

Apart from wet chemistry methods, the exposure of a surface to oxygen plasma yields hydroxyl groups as well. In a plasma chamber, a low-pressure gas is irradiated by kHz to MHz waves to excite and ionize its atoms. In consequence, the UV-radiation emitted by the gas can photolyse typical organic bonds and remove surface contaminations. Additionally, reactive oxygen species such as  $\text{O}_2^+$ ,  $\text{O}_2^-$ ,  $\text{O}_3$  or  $\text{O}$  either oxidize the surface as well or bind dissociated components with low vapor pressure. During an evacuation in the process, these molecules are removed from the chamber intrinsically. [23]

## 2.2.2. Silane Chemistry

By the use of silane chemistry a surface is rendered organofunctional with alkoxy silane molecules. Since glass, silicon, alumina, titania, and quartz surfaces, as well as other metal oxide interfaces, are rich in hydroxyl groups, silanes are particularly useful for modifying these materials. [24]

The general formula for a silane coupling agent (Fig. 4) typically shows the two classes of functionality. X is a hydrolyzable group typically alkoxy, acyloxy, halogen or amine.

Following hydrolysis, a reactive silanol group is formed, which can condense with other silanol groups to form siloxane linkages. (Fig. 5) Stable condensation products are also formed with other oxides such as those of aluminum, zirconium, tin, titanium, and nickel. Less stable bonds are formed with oxides of boron, iron, and carbon, whereas alkali metal oxides and carbonates do not form stable bonds with siloxanes at all. The R group (Fig. 4) is a nonhydrolyzable organic radical that may possess a functionality that imparts desired characteristics. One of the more common silanes is (3-aminopropyl)triethoxysilane (APTES), where the X group consists of an  $-\text{O}-\text{CH}_2-\text{CH}_3$  (ethoxy) group, the organic rest R is substituted by an  $-\text{NH}_2$  (amine) and the 3  $-\text{CH}_2-$  (methylene) groups alter n to 3. [25]

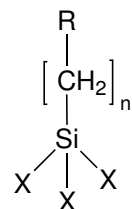


**Figure 4: Trialkoxysilane**  
Structure of a typical trialkoxysilane, X: hydrolyzable group, R: non-hydrolyzable organic radical, n: methylene chain-length

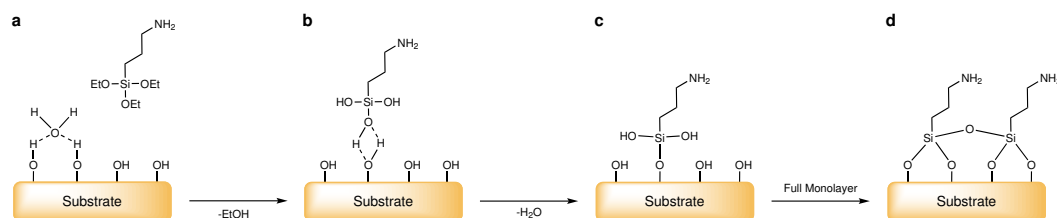


**Figure 5: APTES Modification of an oxidized surface**

a Before the condensation reaction, the oxidized surface forms hydrogen bonds with water molecules. The silane molecules are in the bulk solution. b The hydrolyzed silanol group adsorbs onto the surface and forms hydrogen bridges with it. c In a condensation reaction, under the loss of water, a covalent bond to the surface forms. d After the SAM assembly the surface is saturated with a covalent-bound, crosslinked silane film. [26]

The final result of reacting an organosilane with a substrate ranges from altering the wetting or adhesion characteristics of the substrate, utilizing the substrate to catalyze chemical transformation at the heterogeneous interface, ordering the interfacial region, and modifying its partition characteristics. Significantly, it includes the ability to effect a

covalent bond between organic and inorganic materials. Especially in optical or biological sensors, silane modifications open a broad range of applications.

However, the silanization reactions bear a few drawbacks which are often neglected. For instance, silane chemistry is strongly temperature and pH-dependent. [27], [28] Further, in a process to build SAMs out of APTES, the reaction has to be catalyzed by water. But already small changes in the water content cause dramatic deviations in layer thickness. [29] Additionally, silanes can crosslink to themselves through possible side reactions. (Fig. 5 D) [30]

### 2.2.3. Carbodiimide Crosslinker Chemistry

The in previous manner produced amine-terminated films by APTES form the basis of many reactions and open the possibility to various applications, such as the direct attachment of biofunctional molecules by carbodiimide crosslinking chemistry.[31] Here,  $-COOH$  (carboxyl) groups are modified by 1-ethyl-3-(3-dimethylaminopropyl)carbodiimide (EDC) and N-hydroxysuccinimide (NHS) to form a stable secondary  $R_1 - CONH - R_2$  (carboxamide) bond with any primary amine.

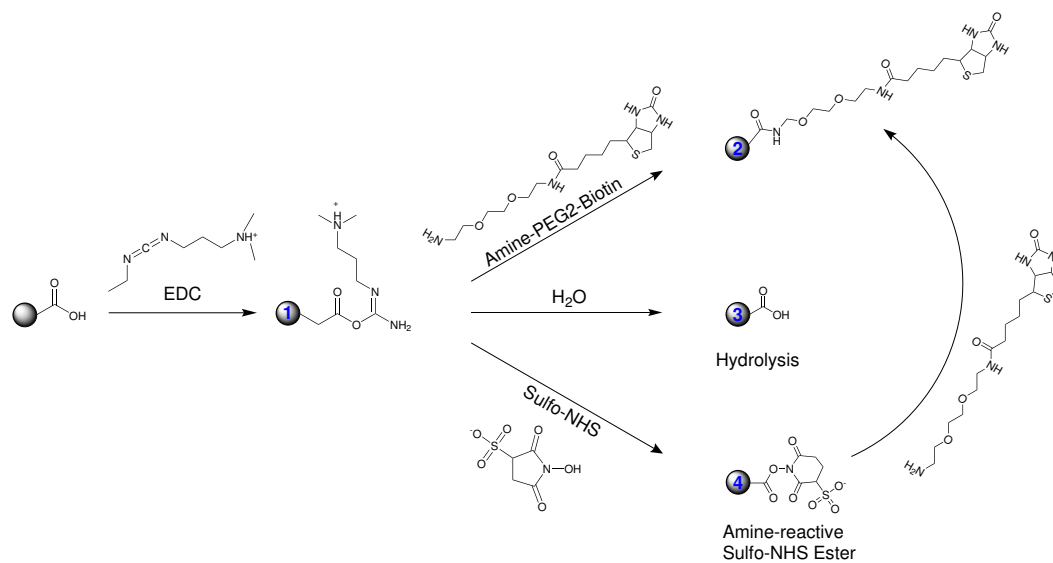


**Figure 6: Carboxyl bead modification with EDC/NHS**

The carboxyl groups bead are activated with EDC to an active O-acylisourea intermediate. This can then either be nucleophilically attacked by a primary amine of the amine-PEG<sub>2</sub>-biotin reactant or - due to its instability - hydrolyzed back to a regenerated carboxyl surface. A present NHS-ester can also displace the O-acylisourea to form a considerably more stable intermediate which then itself reacts with any primary amine.

The general reaction mechanism is depicted in Fig. 6 for the example of a microbead surface, but it can equivalently be applied to any other modified surface or molecule. The initial carboxyl group is esterified by EDC to an active o-acylisourea intermediate and leaves rapidly upon nucleophilic attack of an amine with release of an iso-urea byproduct. A zero-length amide linkage is formed. (Fig. 6, 1->4) Sulphydryl and hydroxyl groups also will react with such active esters, but the products of such reactions, thioesters and esters, are relatively unstable compared to an carboxamide bond. (Fig. 6, 1)

However, this reactive complex is slow to react with amines and can hydrolyze in aqueous solutions, having a rate constant measured in seconds. If the target amine does not find the active carboxyl before it hydrolyzes (Fig. 6, 3), the desired coupling cannot occur. This is especially a problem when the target molecule is in low concentration compared to water, as in the case of protein molecules. Notwithstanding, forming a NHS ester intermediate from the reaction of the hydroxyl group on NHS with the EDC active-ester complex increases the resultant amide bond formation remarkably. (Fig. 6, 3->4) [32]

Another critical point in carbodiimide chemistry is the solubility of the compounds. EDC, NHS and N-hydroxysulfosuccinimide (sulfo-NHS) are soluble in aqueous and organic solvents. Nevertheless, activation with non-sulfonate NHS decreases water-solubility of the modified carboxylate molecule, while activation with sulfo-NHS preserves or increases its water-solubility by virtue of the charged sulfonate group. [33]

## 2.2.4. Microscopic Particle Surface Physics

### 2.2.5. The Biotin-Avidin-System

Until now, the interaction of the homotetrameric protein avidin and its ligand biotin forms one of the strongest known non-covalent bonds in biological systems characterized by a dissociation constant ( $K_d$ ) in the range of  $10^{-15}$  M.[34] First isolated from chicken egg white, it became a standard to use in biotechnology when researchers found a similar bacteria protein - streptavidin - in *Streptomyces* strains.[35] However, the charged glycoprotein avidin exhibits unspecific binding in some assays in comparison to streptavidin. Therefor, several companies developed deglycosylated forms of avidin with a neutral isoelectric points to minimize unspecificity. (NeutrAvidin, Extravidin, NeutraLite) In recent studies, a mutant streptavidin called "Traptavidin" exhibited an even 10 times dissociation rate.[36] As discovered in the early 1990s, biotin is bound inside a highly stable  $\beta$ -barrel structure, and stabilized by hydrogen bonds and van der Waals forces.[37] In a unique mechanism, a side group of biotin (valerate) binds to a neighboring monomer of streptavidin and therefor stabilizes the dimer complex intrinsically.[38], [39] From a thermodynamical point-of-view, the interaction of the vitamin and protein is described by a total free binding energy of  $300 \text{ kJ mol}^{-1}$  to  $330 \text{ kJ mol}^{-1}$  for a tetrameric protein. [39] All these aspects lead to a significant rupture force for the biotin-release of 250 pN.[40]

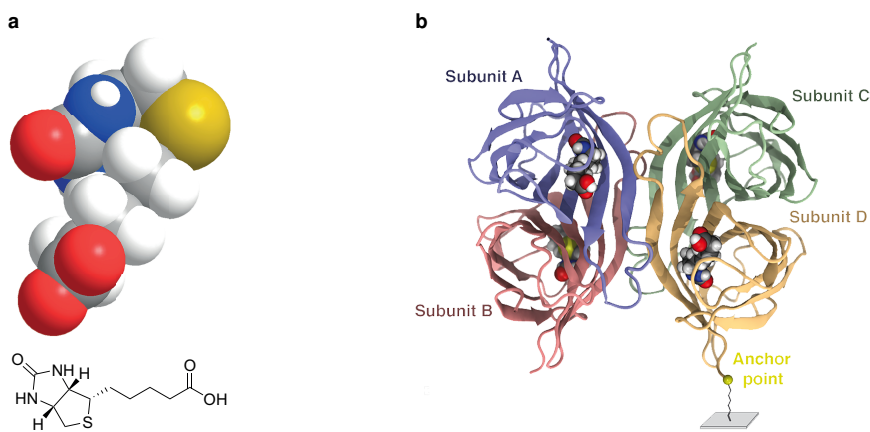


**Figure 7: Functional Structures of Biotin and Streptavidin**

(a) Biotin chemical structure, (b) Homotetrameric Streptavidin with the anchor point at one terminus.[41]

## 2.3. Magnetoresistive Sensing

Short intro in GMR Short intro over MRCyte

### 3. Materials and Methods

#### 3.1. Magnetic Sensor Device

##### 3.1.1. Assembly of Sensor

The fabrication of a microfluidic device on various substrates and layouts consists of two parallelizable workflows. First, the GMR-sensor chip (Sensitec) is assembled into a custom designed PCB (Piu-Printex) by double sided adhesive tape and a square glass slide (25 mmx25 mm, Thermo Scientific) at the bottom. A connection in between was formed by wedge wire bonding (HB10, TPT) which bonded 25 µm thick gold wire to the respective gold bond pads. The optimal parameters are listed in table 1. However, cru-

Parameters	Bond 1	Bond 2
Ultrasonic Power	250	300
Time / ms	200	200
Force / mN	250	300

Table 1: Wirebonding Parameters

cial for successful wire bonding is the optimal hole shape in the welding tool. Therefore, it was cleaned when bonds failed for no obvious reason by removing the gold wire and dipping the tip of the wedge into isopropanol (IPA). Then, *Test USG* was alternated for several seconds in multiple iterations. Afterwards, the wedge was blown dry from all sides with pressurized air and the wire was loaded back into the tool. After wire bonding, the manufactured sensors were placed in a wafer shipper box and stored in a dust free environment upon further use.

##### 3.1.2. Design and Fabrication of Microfluidics

In the second workflow, a microfluidic channel was manufactured via photo- and soft-lithography and bonded to the produced sensors from 3.1.1.

##### Development of Layout Patterning of Photoresist

3" (100) silicon wafers (Si-Mat) were dehumidified in a drying oven (UN30, Memmert) for 2 h at 150 °C to 180 °C. Then, immediately after they reached room temperature, they were placed centered inside a wafer spinner (WS-650-23B, Laurell Technologies).

Foto of setup with arrows to necessary parts  
Microscope  
Stages PEEK  
holder Helmholtz  
coils Kepco  
MFLI DAQ Los  
because of reduced velocity and magnetic drag Different produced GMF stacks Wheatstone Bridge setup Magnet alignment

layout design, hier noch die mänder und verengungen oder den kappt 150u wafer?

For the desired layer thicknesses 2 mL to 3 mL SU8-30XX (Microchem) were poured carefully onto the center of the wafer and the following program was carried out:

1. 500 rpm for 10 s at  $100 \text{ rpm s}^{-1}$
2. 3000 rpm for 30 s at  $300 \text{ rpm s}^{-1}$
3. Ramp down at  $300 \text{ rpm s}^{-1}$

Upon finish, the wafer was gripped outermost with wafer tweezers and soft-baked on a hot plate (super nova+, Thermo Scientific) for 5 min at 65 °C and at least 10 min at 90 °C. The optimal duration was determined if the gently touched resist did not stick to the tweezers. To prevent cracks in the resist caused by a fast temperature change, the wafer was cooled on the hotplate to room temperature. Such processed wafers were stored for a maximum of 4 weeks in a light-tight storage box.

To pattern the resist, the i-Line of a laser lithograph (Dilase 250, Kloe) was used. In preparation of the writing layout a AutoCADz \*.dxf-file with only one layer of polylines was imported to the program “Kloe Design”, converted to contours and subsequently to polygons. For the filling a spot-size equivalent to the minimal structure resolution (as measured in Hicsanmaz [42]) and an overlap of at least 50 % was chosen. The writing trajectories were displayed for a last control before the export to ensure only closed contours. Finally the contour and filling were exported into separate files.

Both files were loaded in this order into the “Kloe Dilase” program. Also the preprocessed wafer was placed inside the laser writer and attached to the vacuumed stage. With the integrated camera the global zero was set to the wafer center by finding the horizontal or vertical edges and adding/subtracting the radius of the wafer ( $3'' \approx \emptyset 76.2 \text{ mm}$ )

### Soft Lithography

The fabricated wafer was placed the center of a 90 cm petri dish. A PDMS mold was created by vigorous mixing of the pre-polymer base with its curing agent (Sygard 184, Dowsil) in a ratio of 10:1 (w/w). For 3" wafers, thin channels were casted from 15 g, normal channels from 20 g PDMS in the petri dish. Gas bubbles were removed from the mixture in a desiccator for 20 min at 2 hPa, and the clear PDMS was cured in an oven (Um, Memmert) for 1 h at 60 °C. After curing, the PDMS mold was released from the petri dish carefully, taken off the wafer and stored in a clean petri dish upon further processing.

### **Bonding of Microfluidics**

Under laminar flow, crosslinked molds were cut into pieces with the respecting single microfluidic ( $\mu$ F) with a razor blade. Holes for in- and outlet were punched through the containing channels with a biopsy puncher (ID 0.5 mm, WellTech). The substrates and  $\mu$ Fs were sonicated in acetone and deionized water (diH<sub>2</sub>O) for 5 min and dried with filtered nitrogen gas (N<sub>2</sub>) completely. For the bonding of PDMS to various substrates different protocols have been established:

### **PDMS Glueing**

Here, a micron-height layer of uncured PDMS was used as an adhesive layer between  $\mu$ F and substrate. Approx. 3 mL were poured onto a 3" wafer and spun down for 5 min at 6000 min<sup>-1</sup>. The microchannel was placed on the substrate by visual control of a stereo microscope (SMZ800, Nikon) with 8-fold magnification. Subsequently, the bonding process could be finished by a 1 h bake at 60 °C or over-night at room temperature.

### **Plasma Bonding**

The respective parts were activated by the exposure to a controlled O<sub>2</sub>-plasma. Bringing the activated surfaces in contact immediately triggers the formation of covalent bonds. First, the acetone-wiped substrates and the microchannels were centered inside the plasma cleaner (Zepto, Diener). Second, vacuum was applied to a final pressure <0.2 hPa. Third, the chamber was flushed with pure O<sub>2</sub> until a chamber pressure from 0.6 hPa to 0.8 hPa had been stabilized. Fourth, the plasma process was executed with 30 W (Power-Potentiometer: 100) for 45 s to 60 s (Time-Potentiometer: 15-20). Upon finish, the chamber was flushed for 5 s and ventilated. Immediately after, the corresponding workpieces were brought into contact and pressed together gently. To ensure a durable bond, the assembled structures were baked for 1 h at 60 °C.

Mass flow equation

### **Reversible Bonding**

To bond the  $\mu$ F to a substrate reversibly and without residues, the channel can be brought into contact with the bottom part without any adhesinon agent. For low-pressure as well as vacuum driven flows, this method is preferable due to its time and work efficiency.

#### **3.1.3. Peripheral Components and Optical Readout**

Each sensor chip was characterized by the hysteresis steepness (equivalent to the sensitivity) and the zero-crossing at half-maximum in a customized setup. Therefore,

the underlying  $32 \times 27 \times 5$  mm NeFeB magnet (NE3227, IBS Magnet) was adjusted on micromanipulator tables (PT, Thorlabs) in three axes to optimize both parameters. Afterwards, PTFE-tubing (ID 0.5 mm, Reichelt Chemietechnik) was connected on the in- and outlet of the microfluidic. A dispensing tip (OD 0.42 mm, Nordson) was connected to the inlet tubing. Initially a 1 mL syringe (ID 4.72 mm, Terumo) was connected with  $\text{dH}_2\text{O}$  or phosphate buffered saline (PBS) and flushed with  $100 \mu\text{L min}^{-1}$  to  $200 \mu\text{L min}^{-1}$  by a syringe pump (Fusion 4000, Chemyx).

### Hysteresis Alignment

For any used GMR-sensor, a characterization of its sensitivity ( $\text{V T}^{-1}$ ) was performed. Therefore, its hysteresis was imposed by two Helmholtz coils ( $L_s = 167 \text{ mH}$ ,  $d = 150 \text{ mm}$ , Brockhaus) generating  $7.8 \text{ mT A}^{-1}$  orthogonal to the easy axis of the GMR which were driven by a voltage-controlled current source (BOP 50-8M, Kepco Inc.) with  $\pm 2 \text{ A}$  at a peak-to-peak voltage ( $V_{pp}$ ) of 20 V. The control voltage was supplied by LabView (2018, 32-bit, National Instruments) supplied by a digital I/O card (USB-6351, National Instruments) in the range of  $-10 \text{ V}$  to  $10 \text{ V}$ . The resulting sensor signal was fed into the current input of a lock-in amplifier ( multi frequency lock-in (MFLI), 5 MHz, Zurich Instruments). Redigitization and processing was carried out by the same digital I/O card and labview program as for the input control.

### Single GMR

The change in resistivity over one whole Wheatstone bridge was measured with a fully-integrated lock-in amplifier ( MFLI, 5 MHz, Zurich Instruments) by a reference peak voltage ( $V_p$ ) of  $100 \text{ mV}$  to  $800 \text{ mV}$ . The reference frequency was chosen randomly in a range of  $100 \pm 25 \text{ kHz}$  such that any harmonics were avoided. The measured differential bridge balance was then demodulated and filtered with a time constant of  $299.7 \mu\text{s}$  by a third order low-pass filter and amplified by the factor 10 000. Subsequently, the processed signal was sampled at  $53.2 \text{ kS s}^{-1}$ , fed into a digital I/O device (USB-6351, National Instruments) with input range  $-10 \text{ V}$  to  $10 \text{ V}$  and processed in LabView.

Additionally, a 40x microscope image (DM2500, Leica Microsystems) was captured by a CCD-camera (Grasshopper3, FLIR) and displayed in real-time to control the experiment.

## Dual GMR

For the measurement of two GMR-sensors simultaneously, the setup from 3.1.3 was duplicated in two different manners. However, the exact same settings in the device control software were crucial for successful measurements. In a first approach, the supply cable of one MFLI was splitted and fed into both sensors, while the bridge balance was evaluated by the same and an additional lock-in, both with the exact same settings. Consequently, the ground pin of the one sensor was the reference also for the other sensor and one ground pin was therefore left floating. This method posed the least cable length and therefore noise, but was also prone to cross-talking between the used BNC-cables respectively -connectors.

circuit/picture of both?

Second, two MFLI's were driven in a master-slave clock synchronization by the Multi-Device Sync function. Therefore, the *trigger out* and *clock out* ports on the backside of the master were connected to the slave's *trigger in* and *clock in* ports. Additionally, the *trigger out* was split by a T-connector piece in order to feed it also back into the master's *trigger in* port.

In both cases, the output of both lock-ins was directed to their respective *AUX 1* ports and connected to another LabView program by the previously mentioned DAQ-card.

## Differential Sensor Setup

In some experiments, two PCBs were stacked with nylon spacers () with various spacings 3 mm, 5 mm and 8 mm between their edges above the permanent magnet. Additionally the outlet tubing of the upper chip was connected to the inlet of the lower chip with the least dead volume possible. The hysteresis was then adjusted for both sensors on various bridges consecutively. Measurements were performed as described in 3.1.3 with two completely independent lock-in amplifiers.

spacers

## GMR Data Analysis

Subsequent data analysis of the acquired streams from both two and one sensor measurements were modified by a custom labview VI to cut the first sample of the stream which was mandatory for the next step. Next, the characteristic signal patterns were detected in the continuous stream by the *GMR\_Tool\_227* by a rolling-mean thresholding method. The resulting *\*\_ana.csv* files were then processed by a custom Matlab script, which in turn computed averages and simple parameters of a single detected signal or

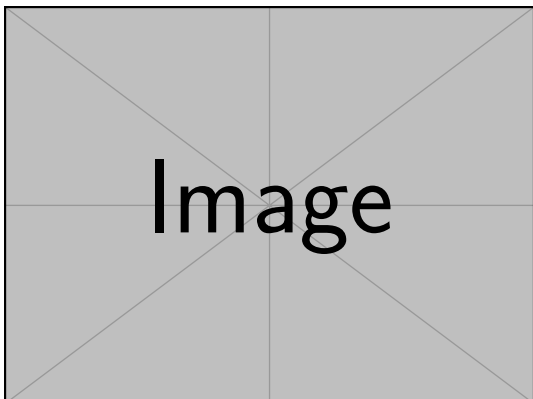


**Figure 8:** Here comes a nice drawing from the stacked pcb setup

whole measured, p.e. the total volume or the signal count therein. The Matlab script saved any analyzed data also in the \*.csv format which was finally plotted in Origin (2020b, [OriginLab](#))

### 3.2. Magnetic Beadometry

Magnetic beads were measured in various manners. First, beads were let rolling over functionalized substrates under microscope control (DM6, Leica) and image acquisition for count and trajectory analyses (LAS X, Leica). Second, beads were measured in buffer in whole blood samples magnetically to determine their concentration in the different samples. The previous concentration measurements were then adapted to functionalized surfaces in order to detect a difference in concentration. In all experiments, PTFE-tubing (ID 0.5 mm, Reichelt Chemietechnik), dispensing tips (OD 0.42 mm, Nordson), 1 mL syringes (ID 4.78 mm, Terumo), a syringe pump (Fusion 4000, Chemyx) and a microfluidic channel with dimension 700  $\mu\text{m} \times 150 \mu\text{m}$  (width x height) were used.

#### 3.2.1. Bead Capture Assay

As prerequisite for the bead capture assay, the concentration of different self-biotinylated particles was determined meticulously in a Neubauer Improved counting chamber as well as by flow cytometry and adjusted between  $1 \mu\text{L}^{-1}$  to  $10 \mu\text{L}^{-1}$  in PBS with Tween 20 (PBS). Further, a GMR sensor was fabricated, loaded unspecifically with  $1 \text{ mg mL}^{-1}$  neutravidin, hysteresis aligned and connected in the single GMR setup (see 3.1.3). As first step, the bead adhesion was determined by finding the minimal flow rate at which non-biotinylated beads were still rolling freely and at second, by finding the maximal flow rate at which biotinylated beads were still notably captured, both by microscope

oberservation and sensor signal analysis. The average flow rate of these two was consequently held constant over all experiments. Subsequently, beads with different surface coverages of biotin were pumped alternately through the channel and over the sensor. The generated data was analyzed after the standard protocol in 3.1.3.

### 3.3. Surface Bio-Functionalization

#### 3.3.1. Surface Activation

To functionalize any silicon containing surface with Si–OH groups which the utilized silane could interact with, multiple surface activation pathways were explored. First, substrates were cleaned in hydrochloric acid (HCl):methanol (MeOH) and H<sub>2</sub>SO<sub>4</sub> before they were immersed in boiling water. Second, surface silanol groups were achieved by piranha immersion. Third a HF dip and fourth a oxygen plasma treatment was tested. For all methods, the following reagents were used: diH<sub>2</sub>O (0.054 µS, Merck MilliQ)), acetone (>99.9 %, VWR), ethanol (EtOH) (absolute, VWR), MeOH (99.8 %, VWR), acetic acid (AcOH) (glacial, VWR), HCl (37 %, Sigma-Aldrich), H<sub>2</sub>SO<sub>4</sub> (95 % to 98 %, VWR), H<sub>2</sub>O<sub>2</sub> (30 % (w/w), Sigma-Aldrich), HF (10 %, VWR)

#### Work Safety Remarks

Before the work with one of the acid solutions was carried out, several safety measures were implemented. As any reacting acid solution becomes very hot immediately due to the exothermic reaction, every container should be placed inside a cooled water or ice bath. Additionally, the beaker as well as concentrated acid flasks should be gripped firmly by a laboratory stand to avoid a tip over. As the reactivity of chemicals is highly temperature-dependent, the solutions was processed further when they had been cooled to  $\leq 80$  °C. It should be also noted that - as in every chemical reaction, but especially ones with H<sub>2</sub>SO<sub>4</sub> and HF - the acid was always poured into the other reactant to avoid splashing and boiling.

#### Plasma Activation

For the plasma activation, process parameters similar to the PDMS bonding technique in ?? were chosen. After initial cleaning via sonication in AcOH and diH<sub>2</sub>O for 5 min each, the substrates were dried in N<sub>2</sub>-gas and placed inside the plasma chamber. The chamber was evacuated to a final pressure <0.2 hPa and then flushed with pure O<sub>2</sub> until a chamber pressure between 0.6 hPa to 0.8 hPa had been stabilized. Fourth, the plasma process was executed with 100 W (Power-Potentiometer: 300) for 300 s (Time-

Potentiometer: ). Upon finish, the chamber was flushed for 5 s and ventilated.

### Hydrochloric-Sulfuric Acid Activation

In order to degrease any glass or Si<sub>3</sub>N<sub>4</sub> surface, a protocol according to Dressick, Dulcey, Georger, *et al.* [43] was used. There, the surfaces were first sonicated in acetone and diH<sub>2</sub>O for 5 min. Afterwards these were immersed in a 1:1 (v/v) solution of HCl:MeOH for >30 min, rinsed with diH<sub>2</sub>O copiously and soaked in H<sub>2</sub>SO<sub>4</sub> for >30 min as well. Then, the samples were rinsed again in deionized water. To form silanol groups on the activated surface, the surfaces were finally immersed in >90 °C heated (Super-Nuova+, Thermo Scientific) diH<sub>2</sub>O for at least 2 h.

### Piranha Activation

In this method, activation was carried out in a 1:7 (v/v) piranha solution at 70 °C for 15 min to 30 min. After treatment, the samples were rinsed carefully with diH<sub>2</sub>O three times.

### Hydrofluoric Acid Activation

For HF activation of Si<sub>3</sub>N<sub>4</sub>, a protocol after Liu, Michalak, Chopra, *et al.* [21] was reproduced. Acetone cleaned samples were immersed in 1 % aqueous HF for 2 min and rinsed with diH<sub>2</sub>O extensively afterwards without letting the surface dry at any time.

### 3.3.2. Chemical Surface Functionalization

Chemically activated surfaces were now coupled with APTES covalently. Therefore an aqueous silane solution was prepared from EtOH with volume fractions of 5 % diH<sub>2</sub>O, 0.5 % aqueous AcOH (pH 4.5) and 1 % APTES in this order. The samples were soaked immediately after their activation in the silane solution. The reaction was carried out for 2 h to 4 h at >40 °C or for 1 h at 70 °C. At finish, all specimens were rinsed with EtOH or sonicated for 5 min in absolute EtOH.

Then, the amine terminated surface modification was enhanced by a carbodiimide conjugation with Poly(acrylic) Acid (PAA) after Andree, Barradas, Nguyen, *et al.* [44]. As above, a reaction consisting of 1 mM 2-(N-morpholino)ethanesulfonic acid (MES) buffer (pH 6) with 1 mg mL<sup>-1</sup> PAA, 6 mM EDC and 3 mM NHS was activated for 15 min on a magnetic stirrer. Subsequently, the prepared samples were immersed in the solution for 1 h on a rotation shaker (VWR). As final cleaning, the slides were rinsed or sonicated for 5 min in diH<sub>2</sub>O and stored in fresh diH<sub>2</sub>O at 4 °C up to 14 d upon further use.

### Tensiometry

All above methods were characterized by a custom built tensiometer and the ImageJ Fiji plugin DropSnake. [45], [46] In an experiment, a substrate was dried by N<sub>2</sub> and placed in the camera focus. Subsequently, a sessile drop of 1 µL was placed in the focus with a micropipette (Eppendorf) without touching the surface. The focus of the camera was adjusted meticulously to gain maximum contrast at the droplet contour and a homogeneously black droplet. Images were then acquired by an USB-microscope pointing in an acute angle onto a drop on the surveyed substrate, while background illumination was provided by a lamp. The images were then cropped, rotated such that the droplet edges were perfectly horizontal and converted to 8-bit grayscale. After preprocessing, the top half contour was outlined by at least 8 points inside the DropSnake plugin and the resulting contact angles were exported.

usb microscope

Background illumination

### 3.3.3. Surface Bioconjugation

A functionalized surface from 3.3.2, was now bonded to a 150 µm microfluidic channel as in 3.1.2 and incubated for at least 5 h, but mostly over night at 7 °C. Upon finish, microfluidic PTFE-tubing (ID 0.5 mm, Reichelt Chemietechnik) was connected to the inlet and outlet with precision tweezers. Then, the channel was equilibrated with 100 µL to 300 µL MES buffer in a syringe (1 mL, Terumo) with a syringe pump (Fusion 100, Chemyx) with 100 µL min<sup>-1</sup>. Then, 50 mM, 100 mM and 300 mM of EDC and NHS were flushed into the channel with the same flow rate after an dissociation time of 10 min. The channel bottom was incubated for 30 min and then washed again with 100 µL MES buffer.

Subsequently, a desired protein was loaded in high concentration (Neutravidin ( 31050, Thermo Scientific): 1 mg mL<sup>-1</sup>, Antibody: 20 µg mL<sup>-1</sup>,) via the tip of a 1 mL syringe or flushed into the channel by vaccuum from a microcentrifuge tube. The functionalized channels were now incubated over night in an ice box. Before use, the µF was washed with 100 µL PBS with 0.02 % nonionic surfactant (Tween 20, Sigma Aldrich) (PBST) for 2 min. Any unreacted binding sites were blocked by a solution of 500 mM ethanolamine hydrochloride (E6133, Sigma-Aldrich) in diH<sub>2</sub>O for 30 min. After another washing step, the functionalized channels were further used for either microscope or magnetic bead-capture experiments.

However, in some experiments focus lay on physisorption rather than on chemisorption.

Therefore, after the bonding of a microfluidic channel to a non-functionalized substrate, the channel was equilibrated as mentioned before with MES buffer (cave: without surfactant). Then it was incubated with a solution containing protein in highest concentration, p.e.  $1 \text{ mg mL}^{-1}$  neutravidin, at  $7^\circ\text{C}$  over night, while infusing and withdrawing a small volume fraction (approx.  $50 \mu\text{L}$ ) continuously by a syringe pump. Upon finish, the tubing was exchanged with a drop of water at the connection and channel was flushed with PBS carefully at  $50 \mu\text{L min}^{-1}$  to avoid any gas bubbles inside the fluidic. It was stored up to 10 d without any notable decrease in functionality.

### 3.3.4. Particle Functionalization

Micro- and nanobeads from different suppliers were used in functionalization experiments but modified after the same procedure according to their surface charge. A positive partial charge from an amine-terminated bead and a negative partial charge from a carboxyl-terminated bead was used to promote different electrostatic interactions with a microchannel's surface. A list of all used particles and their respective parameters are depicted in table 2.

#### Amine-terminated Beads

For amine beads, NHS-Biotin (203118, Sigma Aldrich) was used for a covalent attachment after the previously mentioned carbodiimide chemistry. Initially, the biotin was dissolved to a concentration of ( $50 \text{ mg mL}^{-1}$ ) in water-free dimethyl sulfoxide (DMSO) and stored upon further use at  $-25^\circ\text{C}$ . The attachment to microbeads was titrated by the molar weight ratio of both reagents and ranged from 10-fold molar excess to a 10 000-fold deficit of biotin over the amine.

In most cases,  $20 \mu\text{L}$  of micromer beads were aliquoted in several microcentrifuge tubes ( $1.5 \text{ mL}$ , Eppendorf) to generate a standard curve of functionalization density later on. NHS-Biotin was diluted to a concentration of  $0.5 \text{ mg mL}^{-1}$  with PBST and vortexed. Then, beads and biotinylation reagent were mixed in the desired ratio thoroughly and incubated for  $1.75 \text{ h}$  at  $8^\circ\text{C}$  in a shaker (Thermomixer, Eppendorf) at  $1400 \text{ min}^{-1}$ .

#### Carboxyl-terminated Beads

The surface of carboxyl-terminated beads was esterified by EDC-NHS chemistry and covalently bound to amine-PEG<sub>2</sub>-biotin (EZ Link, Thermo Scientific). First, the bead buffer was exchanged to MES buffer with Tween 20 (MES) with one washing step by

Supplier	Brand Name	d ( $\mu\text{m}$ )	Functionalization	Surface Charge ( $\mu\text{mol g}^{-1}$ )	Magnetic Particle Moment ( $\text{A m}^2$ )
micromod	micromer	8	amine	2.0	0
micromod	micromer-M	8	amine	1.0	$>1.12 \times 10^{-12}$
micromod	micromer	8	carboxyl	2.0	0
micromod	micromer-M	8	carboxyl	1.0	$>1.12 \times 10^{-12}$
invitrogen	Dynabead M280	2.8	streptavidin	0.65-0.90	N.A.
invitrogen	Dynabeads MyOne C1	1.05	streptavidin	>2.5	N.A.
Ocean Nanotec	SV0050	0.05	streptavidin	N.A.	N.A.
micromod	BNF-Dextran-redF	0.1	streptavidin	0.2	$>1.27 \times 10^{-16}$
micromod	nanomag-D-spio	0.1	streptavidin	0.02-0.04	$>5.5 \times 10^{-17}$

**Table 2:** Properties of the used microbeads and magnetic nanoparticles (MNPs).

centrifugation (as in 3.3.4) to a final bead concentration of  $5 \text{ mg mL}^{-1}$ .  $100 \text{ mM}$  EDC in diH<sub>2</sub>O and  $50 \text{ mM}$  NHS in DMSO were prepared and added to the bead solution to a final concentration of  $25 \text{ mM}$  and  $12.5 \text{ mM}$  each. The suspension was reacted for  $30 \text{ min}$  on a shaker at  $1400 \text{ min}^{-1}$  and washed once with MEST buffer. Then, amine-PEG<sub>2</sub>-biotin was added from 10-fold molar excess to a 10 000-fold deficit of biotin over the amine and volume adjusted. The samples were incubated on a shaker for  $1.75 \text{ h}$  at  $8^\circ\text{C}$  in a shaker at  $1400 \text{ min}^{-1}$ .

### Post-Processing and Characterization of Beads

After the incubation, the beads were washed either magnetically or via pelleting. Magnetic washing was carried out in a magnet stand (, where the beads were separated for  $2 \text{ min}$  and then washed 3 times with  $500 \mu\text{L}$  to  $1000 \mu\text{L}$  PBST. Pellet washing was conducted three times in a table centrifuge (Fresco 17, Thermo Scientific) at  $800 \times g$  to  $1200 \times g$  for  $10 \text{ min}$ . The supernatant was discarded and the pellet was dissolved in

Which company?

500  $\mu\text{L}$  to 1000  $\mu\text{L}$  PBST. After both washing procedures, the beads were resuspended in 100  $\mu\text{L}$  MACS running buffer (MACS) or PBST and stored at 4 °C.

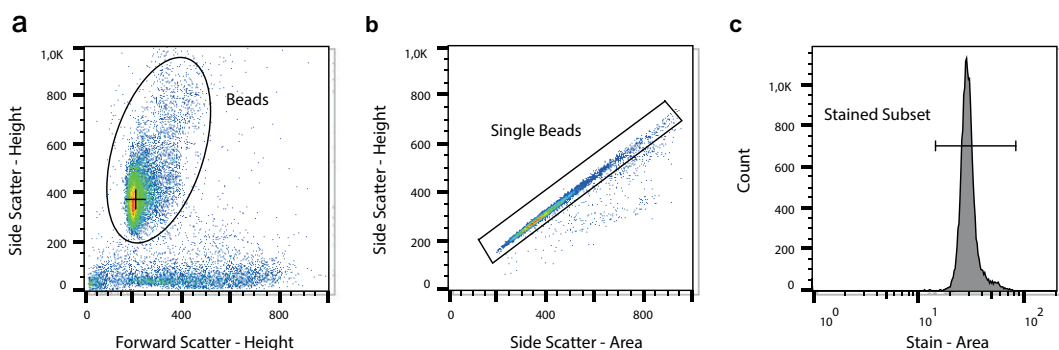


**Figure 9: Gating Strategy for Biotinylated Beads**

- a, In the forward-side-scatter plot, the general bead population with high side scatter is selected from the background.
- b, Single beads are differentiated by their sphericity, their ratio of height:area in the side scatter. Points on the line through the origin are spherical.
- c, The stained subset in the respective color is now selected and the median fluorescence intensity (MFI) as well as the coefficient of variance (CV) is computed.

Characterization of any surface modification was done via fluorescence-flow cytometry or -microscopy. 30 000 beads to 60 000 beads were diluted to 20  $\mu\text{L}$  and incubated with 100 ng streptavidin-atto488 (49937, Sigma Aldrich) or Anti-Biotin-PE ( Miltenyi) for 30 min at 8 °C in a shaker. The beads were then diluted to a final volume of 100  $\mu\text{L}$ , transferred to a 96-well plate (TPP) and measured in the autosampler of a flow cytometer (MACS Quant Analyzer 10, Miltenyi). Following parameters were held constant over all measurements: *Flow Rate*: High, *Mix Sample*: Strong, *Mode*: Standard, *Uptake/Sample Volume*: 100  $\mu\text{L}$ . The photmultiplier voltages of forward and side scatter were lowered in most experiments by 10 V and 120 V respectively due to the homogeneous and reflective nature of the particles. Data analysis was performed by FlowJo (10.6.2, Becton Dickinson) after a gating strategy which is depicted in Fig. 9. For fluorescence microscopy, the beads were stained with streptavidin-atto488 after the same procedure and imaged statically on a covered microscope slide at an exposure time of >100 000  $\mu\text{s}$  and a gain >15. Images were then processed by Fiji. In both measurements, the resulting data was plotted in Origin (2020b, OriginLab).

#### Coating of Biofunctionalized Non-Magnetic Beads with Magnetic Nanoparticles

The biotinylated, non-magnetic microbeads (Table 2) were coated covalently with different MNPs in order to establish a bead-side titration of binding sites. Therefore, 5 mg mL<sup>-1</sup> biotinylated beads in PBST were equilibrated for 10 min and mixed with 7.5  $\mu\text{g}$  BNF-dextran-redF-streptavidin / nanomag-D-spio, 6  $\mu\text{g}$  of SV0050 or 10  $\mu\text{g}$  Dyn-

abeads C1 over night on a shaker. Afterwards, the supernatants were exchanged twice by careful centrifugation to avoid sedimentation of the nanoparticles.

## 4. Results

test,test

### 4.1. Virtual Prototyping of Cell Signals

#### 4.1.1. Numerical investigation of immunomagnetic label density and size on quantitative magnetoresistive sensing of single cells and cell aggregates

Signal Similarity For Cells With Varying Bead Coverages

Cross-Correlation between single dipole with sum magentic moment and surface covered with randomly distributed magnetic particles

simulation of cell rolling velocity and forces

#### 4.1.2. Single Cell Signal

#### 4.1.3. Cell Aggregates

### 4.2. Reference Bead Surface Functionalization

#### 4.2.1. Amine-Surface Biotinylation

Streptavidin-Atto488 reference calibration Anti-Biotin-PE working? BNF-Dextran-Streptavidin unspecific binding?

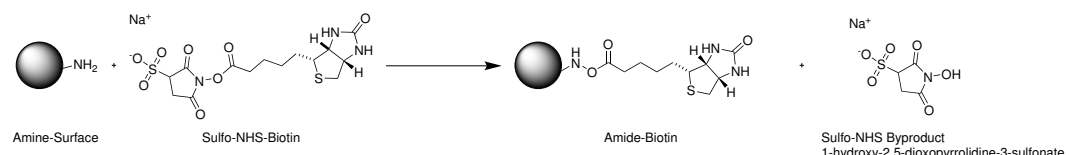


**Figure 10: Amine bead modification with Sulfo-NHS-Biotin**

An amine terminated bead is incubated with sulfo-NHS-Biotin to cover its surface by amide-Biotin. As byproduct the sulfo-NHS-ester 1-hydroxy-2,5-dioxopyrrolidine-3-sulfonate splits off.

#### Magnetic Polystyrene Bead

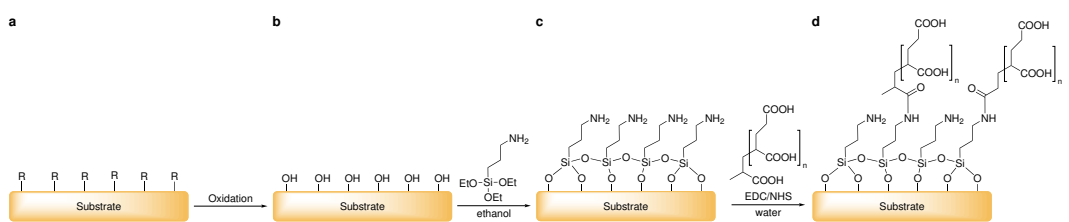


**Figure 11: General process chain of chemical surface modification**

Any substrate with various surface groups  $R$  (a) is oxidized to exhibit hydroxyl groups.(b). Then a silane SAM is attached (c) and subsequently modified by carbodiimide chemistry with PAA. (d)



**Non-Magnetic Polystyrene Bead**



- 4.2.2. Carboxy-Surface Biotinylation**
- 4.2.3. Surface Magnetization of Biofunctionalized Beads**
- 4.3. Concentration Measurements in MRCyte**

Results with  
ocean nanotec  
and bnf

#### **4.3.1. Count Stability**

Measurement over 1h Measurement of Syringe Tubing Losses

#### **4.3.2. Calibration of Flow Field**

##### **4.3.3. Differential Counting Setup**

Sensitivity Calibration

Concentration Measurements



## 4.4. Surface Modification and Biofunctionalization of the Sensor Chip Substrate

### 4.4.1. Physisorption

Quantification in Plate Reader Trial with Neutravidin + Sensor (Esthis Versuch)

#### **4.4.2. Covalent Attachment**

**Plasma-Based Approach**

**Water-Based Approach**

Sonicate in Acetone and Water 5' 1:1 HCl:Methanol H<sub>2</sub>SO<sub>4</sub> Treat for 30 min in light  
boiling water

## 5. Discussion

test,test

Contact angle for silanization of surface methods more useful -> should be 1st approach for characterization

Anti-Biotin-PE working? BNF-Dextran-Streptavidin unspecific binding? electrostatic surface interaction evidence covalent binding?

gas bubbles, adsorption decrease, tubing exchange

## 6. Outlook

# List of Abbreviations

## Symbols

$\tau$ - surface stress tensor .....
$\eta$ - dynamic viscosity .....
$\mu F$ - microfluidic .....
$\rho$ - density .....
$\sum_i f_i$ - body forces .....

## A

AAF - artificial Anti-Ferromagnet .....
AcOH - acetic acid .....
AFM - Anti-Ferromagnetism .....
amine - $-NH_2$ .....
APTES - (3-aminopropyl)triethoxysilane .....

## C

carboxamide - $R_1 - CONH - R_2$ .....
carboxyl - $-COOH$ .....
CV - coefficient of variance .....

## D

diH <sub>2</sub> O - deionized water .....
DMSO - dimethyl sulfoxide .....

## E

EDC - 1-ethyl-3-(3-dimethylaminopropyl)carbodiimide .....
ethoxy - $-O - CH_2 - CH_3$ .....
EtOH - ethanol .....

## F

FM - Ferrimagnetism .....
FWHM - full width at half maximum .....

## G

GMR - giant magneto resistance .....

## H

$\text{H}_2\text{O}_2$  - hydrogen peroxide .....

$\text{H}_2\text{SO}_5$  - Caro's acid.....

$\text{H}_2\text{SO}_4$  - sulfuric acid.....

HCl - hydrochloric acid .....

HF - hydrofluoric acid.....

hydroxyl - –OH .....

## I

IPA - isopropanol .....

## K

$K_d$  - dissociation constant.....

## M

MACS - MACS running buffer.....

MeOH - methanol.....

MES - 2-(N-morpholino)ethanesulfonic acid.....

MEST - MES buffer with Tween 20.....

methylene - –CH<sub>2</sub> – .....

MFI - median fluorescence intensity.....

MFLI - multi frequency lock-in .....

MNP - magnetic nanoparticle.....

## N

$\text{N}_2$  - nitrogen gas .....

NFM - non-ferro-magnetic.....

NHS - N-hydroxysuccinimide.....

## O

$\text{O}_2$  - oxygen gas .....

## P

PAA - Poly(acrylic) Acid.....

PBS - phosphate buffered saline .....

PBST - PBS with Tween 20.....

PCB - printed circuit board.....

PDMS - poly(dimethyl siloxane).....

PM - Paramagnetism .....

## S

SAM - self-assembled monolayer .....

$\text{Si}_3\text{N}_4$  - silicon nitride.....

silanol - Si–OH.....

siloxane - Si–O–Si.....

SMA - styrene maleic anhydride.....

SPM - superparamagnetism .....

sulfo-NHS - N-hydroxysulfosuccinimide .....

## U

u - flow field.....

## V

$V_{pp}$  - peak-to-peak voltage.....

$V_p$  - peak voltage.....



# List of Figures

<b>1</b>	<b>Syringe Pump error sources</b>	
	Set flow rate: — , Real Flow Rate: — <b>a</b> , Transient step answer of a syringe pump through a microtube with 254 µm inner diameter. <b>b</b> , Steady state flow rate error around the desired 5 µL min <sup>-1</sup> dispensing rate. A sinusoidal behaviour caused by the microstepping can be observed. [6]	7
<b>2</b>	<b>Different substrate surfaces: glass and PDMS</b>	
	Surface groups and internal structure of quartz glass ( <b>a</b> ) and PDMS ( <b>b</b> ). After an oxidation step, the methyl groups are changed to hydroxyl. . . . .	10
<b>3</b>	<b>Proposed modification of Si<sub>3</sub>N<sub>4</sub> with HF</b>	
	.....	12
<b>4</b>	<b>Trialkoxysilane</b>	
	Structure of a typical trialkoxysilane, X: hydrolyzable group, R: non-hydrolyzable organic radical, n: methylene chain-length . . . . .	13
<b>5</b>	<b>APTES Modification of an oxidized surface</b>	
	<b>a</b> Before the condensation reaction, the oxidized surface forms hydrogen bonds with water molecules. The silane molecules are in the bulk solution. <b>b</b> The hydrolyzed silanol group adsorbs onto the surface and forms hydrogen bridges with it. <b>c</b> In a condensation reaction, under the loss of water, a covalent bond to the surface forms. <b>d</b> After the SAM assembly the surface is saturated with a covalent-bound, crosslinked silane film. [26]	13
<b>6</b>	<b>Carboxyl bead modification with EDC/NHS</b>	
	The carboxy groups bead are activated with EDC to an active O-acylisourea intermediate. This can then either be nucleophilically attacked by a primary amine of the amine-PEG <sub>2</sub> -biotin reactant or - due to its instability - hydrolyzed back to a regenerated carboxyl surface. A present NHS-ester can also displace the O-acylisourea to form a considerably more stable intermediate which then itself reacts with any primary amine. . . . .	14

<b>7</b>	<b>Functional Structures of Biotin and Streptavidin</b>	
(a)	Biotin chemical structure, (b) Homotetrameric Streptavidin with the anchor point at one terminus.[41]	16
8	Here comes a nice drawing from the stacked pcb setup	22
<b>9</b>	<b>Gating Strategy for Biotinylated Beads</b>	
a,	In the forward-side-scatter plot, the general bead population with high side scatter is selected from the background. b, Single beads are differentiated by their sphericity, their ratio of height:area in the side scatter. Points on the line through the origin are spherical. c, The stained subset in the respective color is now selected and the MFI as well as the CV is computed.	28
<b>10</b>	<b>Amine bead modification with Sulfo-NHS-Biotin</b>	
	An amine terminated bead is incubated with sulfo-NHS-Biotin to cover its surface by amide-Biotin. As byproduct the sulfo-NHS-ester 1-hydroxy-2,5-dioxopyrrolidine-3-sulfonate splits off.	30
<b>11</b>	<b>General process chain of chemical surface modification</b>	
	Any substrate with various surface groups R (a) is oxidized to exhibit hydroxyl groups.(b). Then a silane SAM is attached (c) and subsequently modified by carbodiimide chemistry with PAA. (d)	31

## List of Tables

1	Wirebonding Parameters . . . . .	17
2	Properties of the used microbeads and MNPs. . . . .	27



# Bibliography

- [1] M. Helou, "Magnetic flow cytometry," PhD Thesis, 2014.
- [2] M. Reisbeck, "Integration und quantitative analyse in der magnetischen durchflusszytometrie," Thesis, 2019.
- [3] J. Brenner, "Superparamagnetic nanoparticles in picoliter droplets for measurements with spin valves," Bachelor Thesis, 2018.
- [4] B. Kirby, *Micro- and Nanoscale Fluid Mechanics*. 2010, ISBN: 9780511760723. DOI: 10.1017/cbo9780511760723.
- [5] H. Bruus, *Theoretical Microfluidics*. Technical University of Denmark: Oxford University Press, 2008, ISBN: 978–0–19–923508–7.
- [6] "Syringe pumps." (2021), [Online]. Available: <https://www.fluigent.com/resources/microfluidic-expertise/what-is-microfluidic/system-comparison-for-microfluidic-applications/>.
- [7] S. K. Mitra and A. A. Saha, "Surface modification, methods," in *Encyclopedia of Microfluidics and Nanofluidics*, Springer US, 2014, pp. 1–9. DOI: 10.1007/978-3-642-27758-0\_1503-2.
- [8] W. Putzbach and N. Ronkainen, "Immobilization techniques in the fabrication of nanomaterial-based electrochemical biosensors: A review," *Sensors*, vol. 13, no. 4, pp. 4811–4840, 2013, ISSN: 1424-8220. DOI: 10.3390/s130404811.
- [9] R. Funari, B. Della Ventura, C. Altucci, A. Offenhäusser, D. Mayer, and R. Velotta, "Single molecule characterization of uv-activated antibodies on gold by atomic force microscopy," *Langmuir*, vol. 32, no. 32, pp. 8084–8091, 2016, ISSN: 0743-7463. DOI: 10.1021/acs.langmuir.6b02218.
- [10] A. Ymeti, J. Kanger, J. Greve, G. Besselink, P. Lambeck, R. Wijn, and R. Heideman, "Integration of microfluidics with a four-channel integrated optical young interferometer immunosensor," *Biosensors and Bioelectronics*, vol. 20, no. 7, pp. 1417–1421, 2005, ISSN: 0956-5663. DOI: <https://doi.org/10.1016/j.bios.2004.04.015>.
- [11] M.-J. Bañuls, R. Puchades, and Á. Maquieira, "Chemical surface modifications for the development of silicon-based label-free integrated optical (io) biosensors: A review," *Analytica Chimica Acta*, vol. 777, pp. 1–16, 2013, ISSN: 0003-2670. DOI: 10.1016/j.aca.2013.01.025.

- [12] N. Lange, "Selective chemical modification of silicon nitride surfaces for novel biosensor application," Thesis, 2017. DOI: <http://dx.doi.org/10.17169/refubium-11275>.
- [13] M. Brunet, D. Aureau, P. Chantraine, F. Guillemot, A. Etcheberry, A. C. Gouget-Laemmel, and F. Ozanam, "Etching and chemical control of the silicon nitride surface," *ACS Applied Materials & Interfaces*, vol. 9, no. 3, pp. 3075–3084, 2017, ISSN: 1944-8244. DOI: 10.1021/acsami.6b12880.
- [14] K. Sekine, Y. Saito, M. Hirayama, and T. Ohmi, "Highly robust ultrathin silicon nitride films grown at low-temperature by microwave-excitation high-density plasma for giga scale integration," *IEEE Transactions on Electron Devices*, vol. 47, no. 7, pp. 1370–1374, 2000, ISSN: 0018-9383. DOI: 10.1109/16.848279.
- [15] M. K. Chaudhury and G. M. Whitesides, "Correlation between surface free energy and surface constitution," *Science*, vol. 255, no. 5049, pp. 1230–1232, 1992, ISSN: 0036-8075. DOI: 10.1126/science.255.5049.1230.
- [16] H. Hillborg, J. Ankner, U. Gedde, G. Smith, H. Yasuda, and K. Wikström, "Crosslinked polydimethylsiloxane exposed to oxygen plasma studied by neutron reflectometry and other surface specific techniques," *Polymer*, vol. 41, no. 18, pp. 6851–6863, 2000, ISSN: 0032-3861. DOI: [https://doi.org/10.1016/S0032-3861\(00\)00039-2](https://doi.org/10.1016/S0032-3861(00)00039-2).
- [17] A. N. Ermakov, I. K. Larin, Y. N. Kozlov, and A. P. Purmal', "The thermodynamic characteristics of hydrogen peroxide in h<sub>2</sub>so<sub>4</sub>-h<sub>2</sub>o solutions," *Russian Journal of Physical Chemistry A*, vol. 80, no. 12, pp. 1895–1901, 2006, ISSN: 0036-0244. DOI: 10.1134/s0036024406120041.
- [18] M. Yashima, Y. Ando, and Y. Tabira, "Crystal structure and electron density of  $\alpha$ -silicon nitride: experimental and theoretical evidence for the covalent bonding and charge transfer," *The Journal of Physical Chemistry B*, vol. 111, no. 14, pp. 3609–3613, 2007, ISSN: 1520-6106. DOI: 10.1021/jp0678507.
- [19] M. Brunet, D. Aureau, P. Chantraine, F. Guillemot, A. Etcheberry, A. C. Gouget-Laemmel, and F. Ozanam, "Etching and chemical control of the silicon nitride surface," *ACS Applied Materials & Interfaces*, vol. 9, no. 3, pp. 3075–3084, 2017, ISSN: 1944-8244. DOI: 10.1021/acsami.6b12880.
- [20] D. J. Michalak, S. R. Amy, D. Aureau, M. Dai, A. Estève, and Y. J. Chabal, "Nanopatterning si(111) surfaces as a selective surface-chemistry route," *Na-*

- ture Materials*, vol. 9, no. 3, pp. 266–271, 2010, ISSN: 1476-1122. DOI: 10 . 1038/nmat2611.
- [21] L. H. Liu, D. J. Michalak, T. P. Chopra, S. P. Pujari, W. Cabrera, D. Dick, J. F. Veyan, R. Hourani, M. D. Halls, H. Zuilhof, and Y. J. Chabal, “Surface etching, chemical modification and characterization of silicon nitride and silicon oxide—selective functionalization of  $\text{Si}_3\text{N}_4$  and  $\text{SiO}_2$ ,” *J Phys Condens Matter*, vol. 28, no. 9, p. 094014, 2016, ISSN: 1361-648X (Electronic) 0953-8984 (Linking). DOI: 10 . 1088/0953-8984/28/9/094014.
- [22] J. Gustavsson, G. Altankov, A. Errachid, J. Samitier, J. A. Planell, and E. Engel, “Surface modifications of silicon nitride for cellular biosensor applications,” *Journal of Materials Science: Materials in Medicine*, vol. 19, no. 4, pp. 1839–1850, 2008, ISSN: 0957-4530. DOI: 10 . 1007/s10856-008-3384-7.
- [23] A. Pizzi and K. Mittal, *Handbook of Adhesive Technology, Revised and Expanded*. Taylor and Francis, 2003, ISBN: 9780203912225.
- [24] B. Seed, “Silanizing glassware,” *Current Protocols in Cell Biology*, vol. 8, no. 1, A.3E.1–A.3E.2, 2000, ISSN: 1934-2500. DOI: 10 . 1002/0471143030 . cba03es08.
- [25] GELEST, *Silane coupling agents*, Catalog, 2014.
- [26] H. Khanjanzadeh, R. Behrooz, N. Bahramifar, S. Pinkl, and W. Gindl-Altmutter, “Application of surface chemical functionalized cellulose nanocrystals to improve the performance of uf adhesives used in wood based composites - mdf type,” *Carbohydrate Polymers*, vol. 206, pp. 11–20, 2019, ISSN: 0144-8617. DOI: <https://doi.org/10.1016/j.carbpol.2018.10.115>.
- [27] N. B. Arnfinnsdottir, C. A. Chapman, R. C. Bailey, A. Aksnes, and B. T. Stokke, “Impact of silanization parameters and antibody immobilization strategy on binding capacity of photonic ring resonators,” *Sensors*, vol. 20, no. 11, 2020, ISSN: 1424-8220. DOI: 10 . 3390/s20113163.
- [28] R. M. Pasternack, S. Rivillon Amy, and Y. J. Chabal, “Attachment of 3-(aminopropyl)triethoxysilane on silicon oxide surfaces: Dependence on solution temperature,” *Langmuir*, vol. 24, no. 22, pp. 12963–12971, 2008, ISSN: 0743-7463. DOI: 10 . 1021/la8024827.
- [29] M. J. Banuls, V. Gonzalez-Pedro, C. A. Barrios, R. Puchades, and A. Maquieira, “Selective chemical modification of silicon nitride/silicon oxide nanostructures to develop label-free biosensors,” *Biosens Bioelectron*, vol. 25, no. 6, pp. 1460–6, 2010, ISSN: 1873-4235 (Electronic) 0956-5663 (Linking). DOI: 10 . 1016/j . bios . 2009 . 10 . 048.

- [30] D. W. Sindorf and G. E. Maciel, "Solid-state nmr studies of the reactions of silica surfaces with polyfunctional chloromethylsilanes and ethoxymethylsilanes," *Journal of the American Chemical Society*, vol. 105, no. 12, pp. 3767–3776, 1983, ISSN: 0002-7863. DOI: 10.1021/ja00350a003.
- [31] *Bioconjugate Techniques*. Elsevier, 2013. DOI: 10.1016/c2009-0-64240-9.
- [32] D. Hoare and D. Koshland, "A method for the quantitative modification and estimation of carboxylic acid groups in proteins," *Journal of Biological Chemistry*, vol. 242, no. 10, pp. 2447–2453, May 1967. DOI: 10.1016/s0021-9258(18)95981-8.
- [33] T. Scientific, *User guide: Nhs and sulfo-nhs*, 2021.
- [34] D. W. Woolley and L. G. Longsworth, "Isolation of an antibiotic factor from egg white.," *Journal of Biological Chemistry*, vol. 142, pp. 285–290, 1942.
- [35] T. Sano and C. R. Cantor, "Expression of a cloned streptavidin gene in escherichia coli.," *Proceedings of the National Academy of Sciences*, vol. 87, no. 1, pp. 142–146, 1990, ISSN: 0027-8424. DOI: 10.1073/pnas.87.1.142.
- [36] C. E. Chivers, E. Crozat, C. Chu, V. T. Moy, D. J. Sherratt, and M. Howarth, "A streptavidin variant with slower biotin dissociation and increased mechanostability," *Nature Methods*, vol. 7, no. 5, pp. 391–393, 2010, ISSN: 1548-7091. DOI: 10.1038/nmeth.1450.
- [37] P. Weber, D. Ohlendorf, J. Wendoloski, and F. Salemme, "Structural origins of high-affinity biotin binding to streptavidin," *Science*, vol. 243, no. 4887, pp. 85–88, 1989, ISSN: 0036-8075. DOI: 10.1126/science.2911722.
- [38] B. Miroux and J. E. Walker, "Over-production of proteins in escherichia coli: Mutant hosts that allow synthesis of some membrane proteins and globular proteins at high levels," *Journal of Molecular Biology*, vol. 260, no. 3, pp. 289–298, 1996, ISSN: 0022-2836. DOI: 10.1006/jmbi.1996.0399.
- [39] S. Miyamoto and P. A. Kollman, "Absolute and relative binding free energy calculations of the interaction of biotin and its analogs with streptavidin using molecular dynamics/free energy perturbation approaches," *Proteins: Structure, Function, and Bioinformatics*, vol. 16, no. 3, pp. 226–245, 1993, ISSN: 0887-3585. DOI: 10.1002/prot.340160303.
- [40] H., B. Heymann, and P. Tavan, "Ligand binding: Molecular mechanics calculation of the streptavidin-biotin rupture force," *Science*, vol. 271, no. 5251, pp. 997–999, 1996, ISSN: 0036-8075. DOI: 10.1126/science.271.5251.997.

- [41] S. M. Sedlak, L. C. Schendel, H. E. Gaub, and R. C. Bernardi, “Streptavidin/biotin: Tethering geometry defines unbinding mechanics,” *Science Advances*, vol. 6, no. 13, 2020. DOI: 10.1126/sciadv.aay5999.
- [42] R. Hicsanmaz, “Setup and assessment of laser lithography for the fabrication and integration of biosensor and microfluidic devices,” Technical University Munich, 2020.
- [43] W. J. Dressick, C. S. Dulcey, J. H. Georger, G. S. Calabrese, and J. M. Calvert, “Covalent binding of pd catalysts to ligating self-assembled monolayer films for selective electroless metal deposition,” *Journal of the Electrochemical Society*, vol. 141, no. 1, pp. 210–220, 1994, ISSN: 0013-4651. DOI: 10.1149/1.2054686.
- [44] K. C. Andree, A. M. Barradas, A. T. Nguyen, A. Mentink, I. Stojanovic, J. Bagerman, J. van Dalum, C. J. van Rijn, and L. W. Terstappen, “Capture of tumor cells on anti-epcam-functionalized poly(acrylic acid)-coated surfaces,” *ACS Appl Mater Interfaces*, vol. 8, no. 23, pp. 14 349–56, 2016, ISSN: 1944-8252 (Electronic) 1944-8244 (Linking). DOI: 10.1021/acsami.6b01241.
- [45] A. Stalder, G. Kulik, D. Sage, L. Barbieri, and P. Hoffmann, “A snake-based approach to accurate determination of both contact points and contact angles,” *Colloids And Surfaces A: Physicochemical And Engineering Aspects*, vol. 286, no. 1-3, pp. 92–103, Sep. 2006.
- [46] J. Schindelin, I. Arganda-Carreras, E. Frise, V. Kaynig, M. Longair, T. Pietzsch, S. Preibisch, C. Rueden, S. Saalfeld, B. Schmid, and et al., “Fiji: An open-source platform for biological-image analysis,” *Nature Methods*, vol. 9, no. 7, pp. 676–682, 2012, ISSN: 1548-7091. DOI: 10.1038/nmeth.2019.
- [47] A. P. Guimarães, *Principles of Nanomagnetism*. Springer International Publishing, 2017. DOI: 10.1007/978-3-319-59409-5.
- [48] micromod Partikeltechnologie GmbH, *Technical data sheet - nanomag®-d-spio 50nm*, 2018.
- [49] M. J. Owen and P. J. Smith, “Plasma treatment of polydimethylsiloxane,” *Journal of Adhesion Science and Technology*, vol. 8, no. 10, pp. 1063–1075, 1994. DOI: 10.1163/156856194X00942.
- [50] C.-G. Stefanita, *Magnetism*. Springer Berlin Heidelberg, 2012. DOI: 10.1007/978-3-642-22977-0.
- [51] K. H. J. Buschow and F. R. de Boer, *Physics of Magnetism and Magnetic Materials*. Springer US, 2003. DOI: 10.1007/b100503.

- [52] G. C. Papaefthymiou, “Nanoparticle magnetism,” *Nano Today*, vol. 4, no. 5, pp. 438–447, Oct. 2009. DOI: 10.1016/j.nantod.2009.08.006.
- [53] P. Gravesen, J. Branebjerg, and O. S. Jensen, “Microfluidics-a review,” *Journal of Micromechanics and Microengineering*, vol. 3, no. 4, pp. 168–182, Dec. 1993. DOI: 10.1088/0960-1317/3/4/002.
- [54] K. C. Andree, A. M. Barradas, A. T. Nguyen, A. Mentink, I. Stojanovic, J. Bagerman, J. van Dalum, C. J. van Rijn, and L. W. Terstappen, “Capture of tumor cells on anti-epcam-functionalized poly(acrylic acid)-coated surfaces,” *ACS Appl Mater Interfaces*, vol. 8, no. 23, pp. 14 349–56, 2016, ISSN: 1944-8252 (Electronic) 1944-8244 (Linking). DOI: 10.1021/acsami.6b01241.
- [55] G. Antonacci, J. Goyvaerts, H. Zhao, B. Baumgartner, B. Lendl, and R. Baets, “Ultra-sensitive refractive index gas sensor with functionalized silicon nitride photonic circuits,” *APL Photonics*, vol. 5, no. 8, 2020, ISSN: 2378-0967. DOI: 10.1063/5.0013577.
- [56] A. Arafat, M. Giesbers, M. Rosso, E. J. R. Sudhölter, K. Schroën, R. G. White, L. Yang, M. R. Linford, and H. Zuilhof, “Covalent biofunctionalization of silicon nitride surfaces,” *Langmuir*, vol. 23, no. 11, pp. 6233–6244, 2007, ISSN: 0743-7463 1520-5827. DOI: 10.1021/la7007045.
- [57] A. Arafat, K. Schroen, L. C. de Smet, E. J. Sudholter, and H. Zuilhof, “Tailor-made functionalization of silicon nitride surfaces,” *J Am Chem Soc*, vol. 126, no. 28, pp. 8600–1, 2004, ISSN: 0002-7863 (Print) 0002-7863 (Linking). DOI: 10.1021/ja0483746.
- [58] B. Baur, G. Steinhoff, J. Hernando, O. Purrucker, M. Tanaka, B. Nickel, M. Stutzmann, and M. Eickhoff, “Chemical functionalization of gan and aln surfaces,” *Applied Physics Letters*, vol. 87, no. 26, p. 263 901, 2005, ISSN: 0003-6951. DOI: 10.1063/1.2150280.
- [59] J. Diao, D. Ren, J. R. Engstrom, and K. H. Lee, “A surface modification strategy on silicon nitride for developing biosensors,” *Anal Biochem*, vol. 343, no. 2, pp. 322–8, 2005, ISSN: 0003-2697 (Print) 0003-2697 (Linking). DOI: 10.1016/j.ab.2005.05.010.
- [60] T. Ghonge, H. Ceylan Koydemir, E. Valera, J. Berger, C. Garcia, N. Nawar, J. Tiao, G. L. Damhorst, A. Ganguli, U. Hassan, A. Ozcan, and R. Bashir, “Smartphone-imaged microfluidic biochip for measuring cd64 expression from whole blood,”

- Analyst*, vol. 144, no. 13, pp. 3925–3935, 2019, ISSN: 1364-5528 (Electronic) 0003-2654 (Linking). DOI: 10.1039/c9an00532c.
- [61] M. Hofstetter, J. Howgate, M. Schmid, S. Schoell, M. Sachsenhauser, D. Adigüzel, M. Stutzmann, I. D. Sharp, and S. Thalhammer, “In vitro bio-functionality of gallium nitride sensors for radiation biophysics,” *Biochemical and Biophysical Research Communications*, vol. 424, no. 2, pp. 348–353, 2012, ISSN: 0006-291X. DOI: 10.1016/j.bbrc.2012.06.142.
- [62] D. Kim and A. E. Herr, “Protein immobilization techniques for microfluidic assays,” *Biomicrofluidics*, vol. 7, no. 4, p. 41501, 2013, ISSN: 1932-1058 (Print) 1932-1058 (Linking). DOI: 10.1063/1.4816934.
- [63] J. Klug, L. A. Pérez, E. A. Coronado, and G. I. Lacconi, “Chemical and electrochemical oxidation of silicon surfaces functionalized with aptes: The role of surface roughness in the aunps anchoring kinetics,” *The Journal of Physical Chemistry C*, vol. 117, no. 21, pp. 11317–11327, 2013, ISSN: 1932-7447 1932-7455. DOI: 10.1021/jp212613f.
- [64] N. Lange, P. M. Dietrich, A. Lippitz, N. Kulak, and W. E. S. Unger, “New azidation methods for the functionalization of silicon nitride and application in copper-catalyzed azide-alkyne cycloaddition (cuaac),” *Surface and Interface Analysis*, vol. 48, no. 7, pp. 621–625, 2016, ISSN: 01422421. DOI: 10.1002/sia.5950.
- [65] A. P. Le Brun, S. A. Holt, D. S. Shah, C. F. Majkrzak, and J. H. Lakey, “The structural orientation of antibody layers bound to engineered biosensor surfaces,” *Biomaterials*, vol. 32, no. 12, pp. 3303–11, 2011, ISSN: 1878-5905 (Electronic) 0142-9612 (Linking). DOI: 10.1016/j.biomaterials.2011.01.026.
- [66] M. E. Marques, A. A. P. Mansur, and H. S. Mansur, “Chemical functionalization of surfaces for building three-dimensional engineered biosensors,” *Applied Surface Science*, vol. 275, pp. 347–360, 2013, ISSN: 01694332. DOI: 10.1016/j.apsusc.2012.12.099.
- [67] A. Psarouli, A. Bourkoula, P. Petrou, K. Misiakos, N. Chaniotakis, and S. Kakabakos, “Covalent binding vs. adsorption of biomolecules on silicon nitride planar waveguides,” *Procedia Engineering*, vol. 25, pp. 350–353, 2011, ISSN: 18777058. DOI: 10.1016/j.proeng.2011.12.086.
- [68] M. Rosso, *Modification of Silicon Nitride and Silicon Carbide Surfaces for Food and Biosensor Applications*. 2009, ISBN: 978-90-8585-379-4.

- [69] P. Saengdee, C. Promptmas, S. Thanapitak, A. Srisuwan, A. Pankiew, N. Thornyanadacha, W. Chaisriratanakul, E. Chaowicharat, and W. Jeamsaksiri, “Optimization of 3-aminopropyltriethoxysilane functionalization on silicon nitride surface for biomolecule immobilization,” *Talanta*, vol. 207, p. 120 305, 2020, ISSN: 1873-3573 (Electronic) 0039-9140 (Linking). DOI: 10.1016/j.talanta.2019.120305.
- [70] S. Tan, L. Wang, J. Yu, C. Hou, R. Jiang, Y. Li, and Q. Liu, “Dna-functionalized silicon nitride nanopores for sequence-specific recognition of dna biosensor,” *Nanoscale Research Letters*, vol. 10, no. 1, 2015, ISSN: 1556-276X. DOI: 10.1186/s11671-015-0909-0.
- [71] T. D. To, A. T. Nguyen, K. N. T. Phan, A. T. T. Truong, T. C. D. Doan, and C. M. Dang, “Modification of silicon nitride surfaces with gopes and aptes for antibody immobilization: Computational and experimental studies,” *Advances in Natural Sciences: Nanoscience and Nanotechnology*, vol. 6, no. 4, 2015, ISSN: 2043-6262. DOI: 10.1088/2043-6262/6/4/045006.
- [72] P. Vermette, T. Gengenbach, U. Divisekera, P. A. Kambouris, H. J. Griesser, and L. Meagher, “Immobilization and surface characterization of neutravidin biotin-binding protein on different hydrogel interlayers,” *Journal of Colloid and Interface Science*, vol. 259, no. 1, pp. 13–26, 2003, ISSN: 00219797. DOI: 10.1016/s0021-9797(02)00185-6.
- [73] C. R. Vistas, A. C. P. Águas, and G. N. M. Ferreira, “Silanization of glass chips—a factorial approach for optimization,” *Applied Surface Science*, vol. 286, pp. 314–318, 2013, ISSN: 01694332. DOI: 10.1016/j.apsusc.2013.09.077.
- [74] C. Wang, Q. Yan, H.-B. Liu, X.-H. Zhou, and S.-J. Xiao, “Different edc/nhs activation mechanisms between paa and pmaa brushes and the following amidation reactions,” *Langmuir*, vol. 27, no. 19, pp. 12 058–12 068, 2011, ISSN: 0743-7463 1520-5827. DOI: 10.1021/la202267p.
- [75] M. Yüce and H. Kurt, “How to make nanobiosensors: Surface modification and characterisation of nanomaterials for biosensing applications,” *RSC Adv.*, vol. 7, no. 78, pp. 49 386–49 403, 2017, ISSN: 2046-2069. DOI: 10.1039/c7ra10479k.
- [76] K. AbuZineh, L. I. Joudeh, B. Al Alwan, S. M. Hamdan, J. S. Merzaban, and S. Habuchi, “Microfluidics-based super-resolution microscopy enables nanoscopic characterization of blood stem cell rolling,” *Sci Adv*, vol. 4, no. 7, eaat5304, 2018, ISSN: 2375-2548 (Electronic) 2375-2548 (Linking). DOI: 10.1126/sciadv.eaat5304.

- [77] B. Alberts, A. Johnson, J. Lewis, D. Morgan, M. Raff, K. Roberts, and P. Walter, *Molecular Biology of the Cell*, ISBN: 0815345240.
- [78] K.-C. Chang and D. A. Hammer, “The forward rate of binding of surface-tethered reactants: Effect of relative motion between two surfaces,” *Biophysical Journal*, vol. 76, no. 3, pp. 1280–1292, 1999, ISSN: 0006-3495. DOI: 10.1016/s0006-3495(99)77291-7.
- [79] R. Cheng, T. Zhu, and L. Mao, “Three-dimensional and analytical modeling of microfluidic particle transport in magnetic fluids,” *Microfluidics and Nanofluidics*, vol. 16, no. 6, pp. 1143–1154, 2013, ISSN: 1613-4982 1613-4990. DOI: 10.1007/s10404-013-1280-z.
- [80] S. Choi, O. Levy, M. B. Coelho, J. M. Cabral, J. M. Karp, and R. Karnik, “A cell rolling cytometer reveals the correlation between mesenchymal stem cell dynamic adhesion and differentiation state,” *Lab Chip*, vol. 14, no. 1, pp. 161–6, 2014, ISSN: 1473-0189 (Electronic) 1473-0189 (Linking). DOI: 10.1039/c3lc50923k.
- [81] M. Dembo, D. C. Torney, K. Saxman, and D. Hammer, “The reaction-limited kinetics of membrane-to-surface adhesion and detachment,” *Proceedings of the Royal Society of London. Series B. Biological Sciences*, vol. 234, no. 1274, pp. 55–83, 1997, ISSN: 0080-4649 2053-9193. DOI: 10.1098/rspb.1988.0038.
- [82] S. J. DeNardo, G. L. DeNardo, A. Natarajan, L. A. Miers, A. R. Foreman, C. Gruettner, G. N. Adamson, and R. Ivkov, “Thermal dosimetry predictive of efficacy of <sup>111</sup>In-chl6 nanoparticle amf-induced thermoablative therapy for human breast cancer in mice,” *J Nucl Med*, vol. 48, no. 3, pp. 437–44, 2007, ISSN: 0161-5505 (Print) 0161-5505 (Linking).
- [83] B. Doffek, “Magnetic flow cytometry for thrombocyte analysis,” Thesis, 2015.
- [84] C. Dong and X. X. Lei, “Biomechanics of cell rolling: Shear flow, cell-surface adhesion, and cell deformability,” *Journal of Biomechanics*, vol. 33, no. 1, pp. 35–43, 2000, ISSN: 00219290. DOI: 10.1016/s0021-9290(99)00174-8.
- [85] M. Ermis, E. Antmen, and V. Hasirci, “Micro and nanofabrication methods to control cell-substrate interactions and cell behavior: A review from the tissue engineering perspective,” *Bioact Mater*, vol. 3, no. 3, pp. 355–369, 2018, ISSN: 2452-199X (Electronic) 2452-199X (Linking). DOI: 10.1016/j.bioactmat.2018.05.005.

- [86] M. A. M. Gijs, "Magnetic bead handling on-chip: New opportunities for analytical applications," *Microfluidics and Nanofluidics*, 2004, ISSN: 1613-4982 1613-4990. DOI: 10.1007/s10404-004-0010-y.
- [87] C. Grüttner, K. Müller, J. Teller, F. Westphal, A. Foreman, and R. Ivkov, "Synthesis and antibody conjugation of magnetic nanoparticles with improved specific power absorption rates for alternating magnetic field cancer therapy," *Journal of Magnetism and Magnetic Materials*, vol. 311, no. 1, pp. 181–186, 2007, ISSN: 03048853. DOI: 10.1016/j.jmmm.2006.10.1151.
- [88] H. Happel John; Brenner, *Low Reynolds number hydrodynamics*, ser. Mechanics of fluids and transport processes. 1981, ISBN: 978-94-009-8352-6. DOI: 10.1007/978-94-009-8352-6.
- [89] U. Hassan, T. Ghonge, J. Reddy B., M. Patel, M. Rappleye, I. Taneja, A. Tanna, R. Healey, N. Manusry, Z. Price, T. Jensen, J. Berger, A. Hasnain, E. Flaughier, S. Liu, B. Davis, J. Kumar, K. White, and R. Bashir, "A point-of-care microfluidic biochip for quantification of cd64 expression from whole blood for sepsis stratification," *Nat Commun*, vol. 8, p. 15949, 2017, ISSN: 2041-1723 (Electronic) 2041-1723 (Linking). DOI: 10.1038/ncomms15949.
- [90] M. Hejazian, W. Li, and N. T. Nguyen, "Lab on a chip for continuous-flow magnetic cell separation," *Lab Chip*, vol. 15, no. 4, pp. 959–70, 2015, ISSN: 1473-0189 (Electronic) 1473-0189 (Linking). DOI: 10.1039/c4lc01422g.
- [91] M. Helou, M. Reisbeck, S. F. Tedde, L. Richter, L. Bär, J. J. Bosch, R. H. Stauber, E. Quandt, and O. Hayden, "Time-of-flight magnetic flow cytometry in whole blood with integrated sample preparation," *Lab on a Chip*, vol. 13, no. 6, 2013, ISSN: 1473-0197 1473-0189. DOI: 10.1039/c3lc41310a.
- [92] Y.-C. Hsiao, R. Khojah, X. Li, A. Kundu, C. Chen, D. B. Gopman, A. C. Chavez, T. Lee, Z. Xiao, A. E. Sepulveda, R. N. Candler, G. P. Carman, D. Di Carlo, and C. S. Lynch, "Capturing magnetic bead-based arrays using perpendicular magnetic anisotropy," *Applied Physics Letters*, vol. 115, no. 8, 2019, ISSN: 0003-6951 1077-3118. DOI: 10.1063/1.5085354.
- [93] J. J. S. Jr, "A method of calibrating helmholtz coils for the measurement of permanent magnets,"
- [94] G. Kokkinis, S. Cardoso, F. Keplinger, and I. Giouroudi, "Microfluidic platform with integrated gmr sensors for quantification of cancer cells," *Sensors and Ac-*

- tuators B: Chemical*, vol. 241, pp. 438–445, 2017, ISSN: 09254005. DOI: 10.1016/j.snb.2016.09.189.
- [95] J. M. Koo and C. Kleinstreuer, “Liquid flow in microchannels: Experimental observations and computational analyses of microfluidics effects,” *Journal of Micromechanics and Microengineering*, vol. 13, no. 5, pp. 568–579, 2003, ISSN: 0960-1317. DOI: PiS0960-1317(03)57671-9Doi10.1088/0960-1317/13/5/307.
- [96] H. G. Kye, B. S. Park, J. M. Lee, M. G. Song, H. G. Song, C. D. Ahrberg, and B. G. Chung, “Dual-neodymium magnet-based microfluidic separation device,” *Sci Rep*, vol. 9, no. 1, p. 9502, 2019, ISSN: 2045-2322 (Electronic) 2045-2322 (Linking). DOI: 10.1038/s41598-019-45929-y.
- [97] T. Li, J. Chen, Y. Han, Z. Ma, and J. Wu, “Study on the characteristic point location of depth average velocity in smooth open channels: Applied to channels with flat or concave boundaries,” *Water*, vol. 12, no. 2, 2020, ISSN: 2073-4441. DOI: 10.3390/w12020430.
- [98] A. Liakopoulos, F. Sofos, and T. E. Karakasidis, “Friction factor in nanochannel flows,” *Microfluidics and Nanofluidics*, vol. 20, no. 1, 2016, ISSN: 1613-4982. DOI: 10.1007/s10404-015-1699-5.
- [99] F. Liu, L. Ni, and J. Zhe, “Lab-on-a-chip electrical multiplexing techniques for cellular and molecular biomarker detection,” *Biomicrofluidics*, vol. 12, no. 2, p. 021501, 2018, ISSN: 1932-1058 (Print) 1932-1058 (Linking). DOI: 10.1063/1.5022168.
- [100] H. Y. Liu, C. Koch, A. Haller, S. A. Joosse, R. Kumar, M. J. Vellekoop, L. J. Horst, L. Keller, A. Babayan, A. V. Failla, J. Jensen, S. Peine, F. Keplinger, H. Fuchs, K. Pantel, and M. Hirtz, “Evaluation of microfluidic ceiling designs for the capture of circulating tumor cells on a microarray platform,” *Adv Biosyst*, vol. 4, no. 2, e1900162, 2020, ISSN: 2366-7478 (Print) 2366-7478 (Linking). DOI: 10.1002/adbi.201900162.
- [101] R. Liu, C. H. Chu, N. Wang, T. Ozkaya-Ahmadov, O. Civelekoglu, D. Lee, A. K. M. Arifuzzman, and A. F. Sarioglu, “Combinatorial immunophenotyping of cell populations with an electronic antibody microarray,” *Small*, vol. 15, no. 51, e1904732, 2019, ISSN: 1613-6829 (Electronic) 1613-6810 (Linking). DOI: 10.1002/smll.201904732.
- [102] J. Loureiro, C. Fermon, M. Pannetier-Lecoeur, G. Arrias, R. Ferreira, S. Cardoso, and P. P. Freitas, “Magnetoresistive detection of magnetic beads flowing at high

- speed in microfluidic channels," *IEEE Transactions on Magnetics*, vol. 45, no. 10, pp. 4873–4876, 2009, ISSN: 0018-9464. DOI: 10.1109/tmag.2009.2026287.
- [103] M. Madadelahi, L. F. Acosta-Soto, S. Hosseini, S. O. Martinez-Chapa, and M. J. Madou, "Mathematical modeling and computational analysis of centrifugal microfluidic platforms: A review," *Lab on a Chip*, vol. 20, no. 8, pp. 1318–1357, 2020, ISSN: 1473-0197. DOI: 10.1039/c9lc00775j.
- [104] R. P. McEver and C. Zhu, "Rolling cell adhesion," *Annu Rev Cell Dev Biol*, vol. 26, pp. 363–96, 2010, ISSN: 1530-8995 (Electronic) 1081-0706 (Linking). DOI: 10.1146/annurev.cellbio.042308.113238.
- [105] D. P. McIntyre, A. Lashkaripour, and D. Densmore, "Rapid and inexpensive microfluidic electrode integration with conductive ink," *Lab on a Chip*, 2020, ISSN: 1473-0197 1473-0189. DOI: 10.1039/d0lc00763c.
- [106] A. Munaz, M. J. A. Shiddiky, and N. T. Nguyen, "Recent advances and current challenges in magnetophoresis based micro magnetofluidics," *Biomicrofluidics*, vol. 12, no. 3, p. 031501, 2018, ISSN: 1932-1058 (Print) 1932-1058 (Linking). DOI: 10.1063/1.5035388.
- [107] N.-T. Nguyen, "Micro-magnetofluidics: Interactions between magnetism and fluid flow on the microscale," *Microfluidics and Nanofluidics*, vol. 12, no. 1-4, pp. 1–16, 2011, ISSN: 1613-4982 1613-4990. DOI: 10.1007/s10404-011-0903-5.
- [108] N. Pamme, "Magnetism and microfluidics," *Lab Chip*, vol. 6, no. 1, pp. 24–38, 2006, ISSN: 1473-0197 (Print) 1473-0189 (Linking). DOI: 10.1039/b513005k.
- [109] J. W. Perthold and C. Oostenbrink, "Simulation of reversible protein–protein binding and calculation of binding free energies using perturbed distance restraints," *Journal of Chemical Theory and Computation*, vol. 13, no. 11, pp. 5697–5708, 2017, ISSN: 1549-9618 1549-9626. DOI: 10.1021/acs.jctc.7b00706.
- [110] A. Pierres, D. Touchard, A.-M. Benoliel, and P. Bongrand, "Dissecting streptavidin-biotin interaction with a laminar flow chamber," *Biophysical Journal*, vol. 82, no. 6, pp. 3214–3223, 2002, ISSN: 0006-3495. DOI: 10.1016/s0006-3495(02)75664-6.
- [111] E. Räth, "Affinity-based cell rolling assays in magnetic flow cytometry," Thesis, 2020.
- [112] M. Reisbeck, M. J. Helou, L. Richter, B. Kappes, O. Friedrich, and O. Hayden, "Magnetic fingerprints of rolling cells for quantitative flow cytometry in whole

- blood," *Scientific Reports*, vol. 6, no. 1, 2016, ISSN: 2045-2322. DOI: 10.1038/srep32838.
- [113] J. Schütt, R. Illing, O. Volkov, T. Kosub, P. N. Granell, H. Nhalil, J. Fassbender, L. Klein, A. Grosz, and D. Makarov, "Two orders of magnitude boost in the detection limit of droplet-based micro-magnetofluidics with planar hall effect sensors," *ACS Omega*, vol. 5, no. 32, pp. 20 609–20 617, 2020, ISSN: 2470-1343 2470-1343. DOI: 10.1021/acsomega.0c02892.
- [114] J. Schütt, D. I. Sandoval Bojorquez, E. Avitabile, E. S. Oliveros Mata, G. Milyukov, J. Colditz, L. G. Delogu, M. Rauner, A. Feldmann, S. Koristka, J. M. Middeke, K. Sockel, J. Fassbender, M. Bachmann, M. Bornhäuser, G. Cuniberti, and L. Baraban, "Nanocytometer for smart analysis of peripheral blood and acute myeloid leukemia: A pilot study," *Nano Letters*, 2020, ISSN: 1530-6984 1530-6992. DOI: 10.1021/acs.nanolett.0c02300.
- [115] F. Shamsipour, A. H. Zarnani, R. Ghods, M. Chamankhah, F. Forouzesh, S. Vafaei, A. A. Bayat, M. M. Akhondi, M. Ali Oghabian, and M. Jeddi-Tehrani, "Conjugation of monoclonal antibodies to super paramagnetic iron oxide nanoparticles for detection of her2/neu antigen on breast cancer cell lines," *Avicenna J Med Biotechnol*, vol. 1, no. 1, pp. 27–31, 2009, ISSN: 2008-2835 (Print) 2008-2835 (Linking).
- [116] S. S. Shevkoplyas, A. C. Siegel, R. M. Westervelt, M. G. Prentiss, and G. M. Whitesides, "The force acting on a superparamagnetic bead due to an applied magnetic field," *Lab Chip*, vol. 7, no. 10, pp. 1294–302, 2007, ISSN: 1473-0197 (Print) 1473-0189 (Linking). DOI: 10.1039/b705045c.
- [117] C. Sommer, "Die Größenabhängigkeit der Gleichgewichtsgeschwindigkeit von Partikeln beim Transport in Mikrokanälen," Thesis, 2014.
- [118] D. Song, R. K. Gupta, and R. P. Chhabra, "Drag on a sphere in Poiseuille flow of shear-thinning power-law fluids," *Industrial and Engineering Chemistry Research*, vol. 50, no. 23, pp. 13 105–13 115, 2011, ISSN: 0888-5885 1520-5045. DOI: 10.1021/ie102120p.
- [119] H. C. Tekin, M. Cornaglia, and M. A. Gijs, "Attomolar protein detection using a magnetic bead surface coverage assay," *Lab Chip*, vol. 13, no. 6, pp. 1053–9, 2013, ISSN: 1473-0189 (Electronic) 1473-0189 (Linking). DOI: 10.1039/c3lc41285g.

- [120] A. E. Urusov, A. V. Petrakova, M. V. Vozniak, A. V. Zherdev, and B. B. Dzantiev, "Rapid immunoenzyme assay of aflatoxin b1 using magnetic nanoparticles," *Sensors (Basel)*, vol. 14, no. 11, pp. 21 843–57, 2014, ISSN: 1424-8220 (Electronic) 1424-8220 (Linking). DOI: 10.3390/s141121843.
- [121] C. Wang, S. Zhao, X. Zhao, L. Chen, Z. Tian, X. Chen, and S. Qin, "A novel wide-range microfluidic dilution device for drug screening," *Biomicrofluidics*, vol. 13, no. 2, p. 024 105, 2019, ISSN: 1932-1058 (Print) 1932-1058 (Linking). DOI: 10.1063/1.5085865.
- [122] H. Wang and Y. Wang, "Measurement of water flow rate in microchannels based on the microfluidic particle image velocimetry," *Measurement*, vol. 42, no. 1, pp. 119–126, 2009, ISSN: 02632241. DOI: 10.1016/j.measurement.2008.04.012.
- [123] H. Watarai and M. Namba, "Capillary magnetophoresis of human blood cells and their magnetophoretic trapping in a flow system," *Journal of Chromatography A*, vol. 961, no. 1, pp. 3–8, 2002, ISSN: 00219673. DOI: 10.1016/s0021-9673(02)00748-3.
- [124] R. Wirix-Speetjens, W. Fyen, X. Kaidong, B. Jo De, and G. Borghs, "A force study of on-chip magnetic particle transport based on tapered conductors," *IEEE Transactions on Magnetics*, vol. 41, no. 10, pp. 4128–4133, 2005, ISSN: 0018-9464. DOI: 10.1109/tmag.2005.855345.
- [125] D. Wu and J. Voldman, "An integrated model for bead-based immunoassays," *Biosensors and Bioelectronics*, vol. 154, 2020, ISSN: 09565663. DOI: 10.1016/j.bios.2020.112070.
- [126] T. Yago, J. Wu, C. D. Wey, A. G. Klopocki, C. Zhu, and R. P. McEver, "Catch bonds govern adhesion through I-selectin at threshold shear," *Journal of Cell Biology*, vol. 166, no. 6, pp. 913–923, 2004, ISSN: 1540-8140. DOI: 10.1083/jcb.200403144.
- [127] R. Yokokawa, Y. Sakai, A. Okonogi, I. Kanno, and H. Kotera, "Force measurement and modeling for motor proteins between microsphere and microfluidic channel surface," ISBN: 978-0-9798064-3-8.
- [128] T. Zhu, D. J. Lichlyter, M. A. Haidekker, and L. Mao, "Analytical model of microfluidic transport of non-magnetic particles in ferrofluids under the influence of a permanent magnet," *Microfluidics and Nanofluidics*, vol. 10, no. 6, pp. 1233–1245, 2011, ISSN: 1613-4982 1613-4990. DOI: 10.1007/s10404-010-0754-5.

- [129] N. Graf, E. Yeğen, A. Lippitz, D. Treu, T. Wirth, and W. E. S. Unger, “Optimization of cleaning and amino-silanization protocols for si wafers to be used as platforms for biochip microarrays by surface analysis (xps, tof-sims and nexasf spectroscopy),” *Surface and Interface Analysis*, vol. 40, no. 3-4, pp. 180–183, 2008, ISSN: 0142-2421. DOI: 10.1002/sia.2621.
- [130] S. Magalhães, L. Alves, B. Medronho, A. C. Fonseca, A. Romano, J. F. Coelho, and M. Norgren, “Brief overview on bio-based adhesives and sealants,” *Polymers*, vol. 11, no. 10, p. 1685, 2019, ISSN: 2073-4360. DOI: 10.3390/polym11101685.
- [131] J. V. Staros, “N-hydroxysulfosuccinimide active esters: Bis(n-hydroxysulfosuccinimide) esters of two dicarboxylic acids are hydrophilic, membrane-impermeant, protein cross-linkers,” *Biochemistry*, vol. 21, no. 17, pp. 3950–3955, 1982, PMID: 7126526. DOI: 10.1021/bi00260a008.
- [132] Y. Eisenberg-Domovich, V. P. Hytönen, M. Wilchek, E. A. Bayer, M. S. Kulomaa, and O. Livnah, “High-resolution crystal structure of an avidin-related protein: insight into high-affinity biotin binding and protein stability,” *Acta Crystallographica Section D*, vol. 61, no. 5, pp. 528–538, May 2005. DOI: 10.1107/S0907444905003914.

# Statement

I declare that I have authored this thesis independently, that I have not used other than the declared sources / resources, and that I have explicitly marked all material which has been quoted either literally or by content from the used sources.

---

Munich, December 4<sup>th</sup>, 2020, Signature